SECTION 1

PHYSICS OF RADIATION DAMAGES AND EFFECTS IN SOLIDS

https://doi.org/10.46813/2022-140-003

UDC 669.017:539.16

HELIUM AND HYDROGEN EFFECTS IN STRUCTURAL MATERIALS FOR NUCLEAR APPLICATIONS

S.A. Karpov, G.D. Tolstolutskaya
National Science Center "Kharkov Institute of Physics and Technology", Kharkiv, Ukraine
E-mail: karpofff@kipt.kharkov.ua

Displacement cascades produce a variety of defects under reactor conditions, but of particular concern is the simultaneous production of helium (He) and hydrogen (H), which enhances the degradation of structural materials. The overall majority of performed studies on helium and hydrogen interactions with materials were based on ion beam irradiation, which served as a convenient tool for the simulation of neutrons exposure over a variety of temperature and dose regimes due to the ability to widely vary and control the irradiation parameters. Experimental investigations of the hydrogen-defect interaction performed by thermal desorption spectroscopy, and the parameters of this interaction obtained by numerical simulations based on diffusion-trapping codes are debated. In this review, we also summarize previous studies on grain boundaries and nanoprecipitate effects on hydrogen transport in metals, as well as the role of hydrogen in the corrosion and cracking of steels. We discuss here issues of helium bubbles formation and some of the evidence for the synergistic effects of hydrogen and helium in the presence of displacement damage, and their influence on irradiation hardening and swelling. Particular attention was devoted to the features of hydrogen interaction with noble-gas bubbles, which were considered on the basis of most recent published data.

INTRODUCTION

Safety of nuclear reactors and economic of nuclear power are determined to high degree by structural materials. One of the main goals of the scientific community focused on nuclear energy is to reduce the degradation of materials in operation. A deep understanding of the physical phenomena and processes causing changes in the materials' properties can make a positive contribution towards this goal.

Structural materials of modern technical devices operate under extreme conditions (high temperatures, high mechanical stresses and high radiation doses). In nuclear reactors and thermonuclear devices, the crystalline structure of materials is constantly undergoing to changes at the atomic level due to nucleation of various kinds of defects. Their appearance dramatically changes the physical properties of materials. Radiation damage of materials involves at least two principal processes: displacement and defect clusters formation representing the reversible process, and the irreversible process of transmutation of elements of the initial material in nuclear reactions [1]. Nuclear reactions in materials produce gaseous impurities, in particular, helium and hydrogen.

A number of results for measuring hydrogen concentrations in LWR irradiated stainless steels (SS) indicated that the measured values ranged from 10 to 200 weight parts per million (wppm). These values did not match the calculated generation amounts from nuclear reactions, therefore hydrogen in LWR-irradiated SSs was suggested to originate from the environment, apparently as a result of corrosion reactions. Helium is produced in nuclear fission and fusion energy systems in amounts ranging from less than one to thousands of atomic parts per million (appm), depending on the neutron spectrum, fluence, and alloy composition. Table 1 shows the amounts of helium and hydrogen produced in various power installations [2].

Table 1

Irradiation parameters in nuclear facilities

Reactor type	Parameters			
	Helium generation rate	Hydrogen generation rate	Dose rate	Used materials
Thermal reactors	~ 280 appm/year	~ 60 appm/year	3 dpa/year	WWER-1000: PVI steel 18Cr10NiTi Pressure vessel 15Cr2NiWA
Fast reactors	20…30 appm/year	–	30…40 dpa/year	Austenitic stainless steels, ferritic/martensitic steels
Fusion reactors	300 appm/year	800 appm/year	20 dpa/year	ferritic/martensitic steels, vanadium alloys
Reactors of IV generation, electro nuclear systems	950…3500 ppm/year	3000…4000 appm/year	5…40 dpa/year	Austenitic stainless steels, ferritic/martensitic steels

Prediction of the material properties under the circumstances of interaction with hydrogen and helium is an important aspect of modern physics and solid-state mechanics [3–6]. Of greatest interest is the study of the features of these gases interaction with metals and their effects on the physical and mechanical properties of the material, since hydrogen and helium, accumulating in the metal parts of the structures, facilitates the appearance of defects, and as a consequence the destruction – the manifestation of the phenomena of cavity swelling [4, 5], high-temperature grain boundary embrittlement and low-temperature hardening [3]. Various aspects of the behavior of ion-implanted helium and hydrogen in metals, their interaction with micro- and macrodefects as well as the defect microstructure evolution were studied in recent decade [7–12].

The effect of hydrogen on the degradation of metals and alloys was reported in a number of detailed reviews [2, 13, 14]. It was postulated that hydrogen dissolved in metals can affect the mechanical properties of the metals through the interactions between hydrogen atoms and material defects. This process involves various phenomena such as hydrogen dissolution and diffusion, its trapping by point defects, dislocations, grain boundaries, etc. [15]. Hydrogen embrittlement (HE) has attracted particular attention since it causes subcritical crack growth in materials, fracture initiation, and loss in mechanical properties such as ductility, toughness and strength. Several hydrogen embrittlement mechanisms have been proposed to explain the HE phenomena, including the hydrogen-enhanced decohesion mechanism, hydrogen-enhanced localized plasticity mechanism, corrosion enhanced plasticity, and so on. Despite great efforts in attempting to understand the mechanisms of failure and in developing potential mitigating solutions, hydrogen-assisted degradation mechanisms are still not completely understood. Meanwhile, in order to reduce the risk of HE for engineering structural materials, surface treatments and microstructural optimization of the alloys have been suggested. The control of diffusible hydrogen can be achieved by introducing strong, harmless traps into material bulk or by preventing the ingress of hydrogen using special barrier coatings.

Due to very low solubility in metals, helium atoms tend to agglomerate into nanosized He bubbles in structural materials. An understanding of He bubbles evolution and their effects on mechanical properties of nuclear materials is one of the key issues in nuclear industry. It has been revealed that He bubbles greatly affect the mechanical properties of metals, causing blistering [16] and swelling [17, 18]. In addition, He-induced embrittlement was shown to be responsible for fracture in metals, particularly at high temperatures via formation of He bubbles along grain boundaries [19, 20].

He-bubbles evolution can be significantly affected in the presence of hydrogen atoms due to the synergistic effects of helium and hydrogen in irradiated materials. It is believed that hydrogen can promote the nucleation and growth of bubbles by enhancing the diffusion of helium atoms/helium vacancy clusters. At the same time, helium bubbles can enhance the retention of hydrogen atoms with the formation of He-H-vacancy complexes [21]. The combined effect of hydrogen and helium may lead to a large amount of volume swelling and further aggravate hardening and embrittlement [22, 23].

In this review, we briefly summarize our previous results and data published by other authors on hydrogen and helium behavior in metals, focusing on recent progress in hydrogen-defect interactions, nucleation and growth of helium bubbles, and synergistic effects of helium and hydrogen in the presence of radiation defects.

1. HYDROGEN

1.1. EFFECT OF RADIATION DEFECTS ON HYDROGEN TRAPPING BEHAVIOR IN STRUCTURAL MATERIALS

Experimental investigations of the hydrogen-defect interaction are often performed by thermal desorption spectroscopy (TDS), and the parameters of the interaction are obtained by fitting numerical calculations based on diffusion-trapping codes to experimental thermal desorption spectra.

Computational evaluation of deuterium desorption within the framework of the diffusion-trapping model [24–26] provides the ability to assess activation energies of de-trapping processes and to associate characteristics of experimental TDS spectra with specific trapping sites in the material. The modeling calculation is a numerical solution [27] for the diffusion of deuterium in the presence of trapping sites.

$$\frac{\partial C(x,t)}{\partial t} = D(T)\frac{\partial^2 C(x,t)}{\partial x^2} - \sum_k \frac{\partial G_k(x,t)}{\partial t} + \phi(x), \quad (1)$$

$$\frac{\partial G_k(x,t)}{\partial t} = 4\pi R_k D(T)\left\{C(x,t)\left[W_k(x,t) - G_k(x,t)/m_k\right] - G_k(x,t) z N_V \exp\left(-\frac{Q_k}{k_Б T}\right)\right\},$$

where C is the concentration of hydrogen in the solution; G_k is the concentration of hydrogen in traps of k-type; R_k is the radius of defect trap; m_k is the number of hydrogen atoms per trap; z is the number of solution sites per host atom; N_V is the atomic density of the host; W_k is trap concentration; φ(x) is the distribution of the hydrogen introduction rate through the depth; Q_k is the binding energy of hydrogen atom with the trap; k_B is Boltzmann's constant, and D(T) = Do exp(-E_m/k_BT) is the deuterium diffusivity.

In order to derive the deuterium trapping parameters, the implantation, diffusion, trapping/de-trapping, and recombination processes that occur during the experiment are simulated to achieve best agreement between experimental data and calculations.

Austenitic stainless steels. Austenitic stainless steels of 300 series and their domestic analogues (18–10 type steels) are widely used as structural materials in generation II and III reactors due to their good creep resistance at high temperature, relatively high strength, corrosion resistance, and good fracture toughness. They

are also considered for many components of future reactors worldwide, including sodium-cooled fast reactors and lead-cooled fast reactors. It is known that hydrogen gas can be stored in irradiated austenitic steels at concentrations significantly in excess of those predicted by Sieverts' law [28]. The retention and accumulation of hydrogen in irradiated materials are most likely caused by the presence of high concentrations of microstructural trapping sites.

A number of studies on the irradiation of austenitic stainless steels with low-energy hydrogen ions clearly demonstrated a significant role of vacancy-type defects on the hydrogen trapping behavior [28–31]. Fig.1 shows experimental data and simulated curves of deuterium thermal desorption from 18Cr10NiTi stainless steel irradiated with 6 keV D^+ to a dose of $1 \cdot 10^{20}$ D/m^2 at room temperature. Insert in Fig. 1 shows the exposure time dependence of deuterium retention in steel at room temperature after irradiation. It is evident, that decrease of deuterium retention is observed for the entire time interval, especially drastically during the first few hours. This indicates a weak deuterium trapping by defects produced in low-energy displacement cascades.

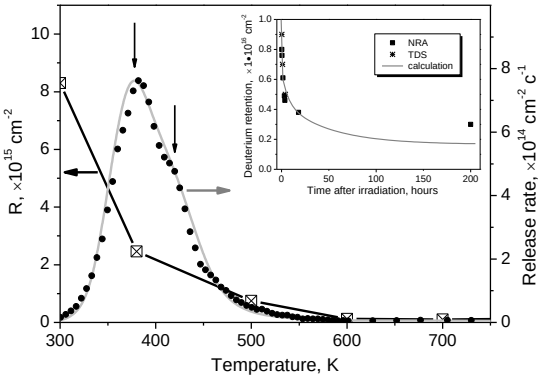

Fig. 1. Experimental (black point) and calculated (grey curve) linear temperature ramp thermal desorption, temperature-dependent areal densities (R) (black curve) and deuterium retention as a function of time (in insert) for 18Cr10NiTi stainless steel samples [32]

Using equations (1), the binding energies of deuterium with radiation defects were derived to be 0.28 and 0.36 eV [32]. According to early suggestions based on effective medium theory, the binding energy of hydrogen with monovacancies in fcc metals ranges from 0.2 to 0.4 eV depending on occupancy of H atoms [33]. Meanwhile, more recent ab initio calculations [34–37] indicated that for monovacancies the value of binding energy is ranged from 0.1 to 0.27 eV depending on the number of hydrogen atoms within the vacancy.

Small vacancy clusters can be considered as defects which can participate in trapping of deuterium, since they are believed to have higher binding energies with a deuterium atom than monovacancies. For instance, results of calculations [35–37] showed that the binding energy of a single H atom with a divacancy in Ni is about 0.4 eV with a slight decreasing of binding energy with increasing of occupancy. In addition, positron annihilation spectroscopy as a technique capable to detect vacancy-type defects with high sensitivity also confirms that the presence of hydrogen atoms plays a crucial role in stabilizing monovacancies/divacancies and can promote the nucleation of vacancy clusters [38].

Ferritic-martensitic steel. Body-centered cubic (bcc) ferritic/martensitic (F/M) steels are considered as one of the most promising materials in advance nuclear reactors [39–41] due to its advantage in high thermal conductivity, good corrosion and radiation resistance comparing with austenitic steels. It is reported that alloys with Cr concentration around 9 at.% have a minimum influence on the shift of the ductile-to-brittle transition temperature among all the Fe-Cr alloys [42].

It is thought that the low solubility and high diffusivity of H in martensite and ferrite relative to austenite may have a significant impact on the H transport behavior in ferritic-martensitic steels. In addition, H diffusion in martensite affected by the presence of dislocations, grain boundaries and retained austenite. Moreover, due to the complexity of martensitic steels, the influence of the individual type of defects is rather difficult to identify [43].

A significant amount of effort has been made with respect to investigations of H-trapping in Fe as the basis of ferritic steels [44–50]. Most research works have focused on the identification of the most favorable position of the atomic H in the lattice or at a defect.

Density functional theory (DFT) studies on H-trapping at vacancies and on formation of vacancy-H clusters in bcc Fe reported trapping energies varying from 0.4 to 0.6 eV. Other DFT calculations with a focus on H-trapping at the edge and screw dislocations suggest a range of the trapping energies from 0.19 to 0.47 eV [47, 48, 50].

In [51], hydrogen trapping characteristics in ion-irradiated F82H (e.g., the trapping energy, the production rate, and the annihilation temperature) were determined. Traps were produced by 0.8 MeV ^{4}He or 0.3 MeV H ion irradiation. Results showed that the traps observed were of one type in each irradiation case and had a trapping energy of 0.66 eV. It was concluded that the F82H trap is an interstitial-type trap associated with dislocation loops produced by the irradiation. Traps are annihilated around 600 K for H irradiation.

It should be noted that in bcc iron overall amount of injected H dramatically drops as temperature increases [44]. The evaluation of H concentration at typical defects using the McLean-Langmuir segregation isotherm at finite temperatures is shown in Fig. 2.

These calculations indicate that H can be evenly distributed between different defects at the near room temperature, suggesting that the effective H-trapping energies at vacancies, grain boundaries (GBs) or dislocations can be virtually indistinguishable from one another. Hence, particular caution should be taken when interpreting experimental and theoretical results in terms of preferred trapping sites.

The effect of vacancy-type defects on hydrogen trapping can be detected using low-energy ion irradiation, since such an impact leads to the generation of predominantly point defects.

Fig. 3 shows the thermal desorption spectrum of hydrogen from EI-852 ferritic-martensitic steel specimens irradiated with 5 keV H^+ ions [9].

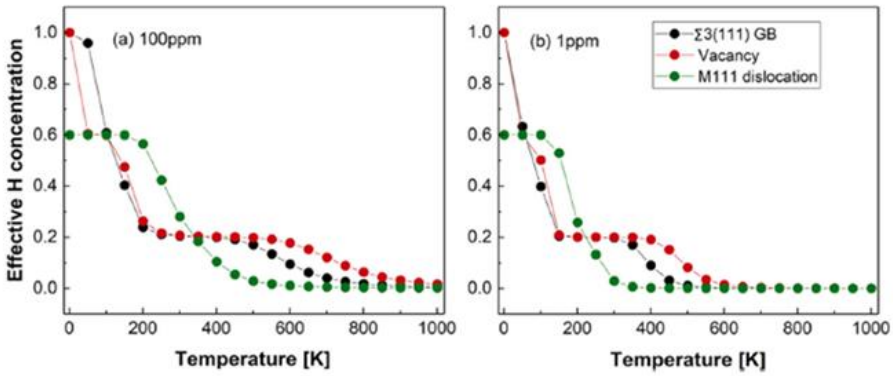

Fig. 2. The temperature dependence of the H concentration at Σ3 (111) GB, M111 dislocation and a vacancy a – for H bulk concentration 100 ppm, b – for H bulk concentration 1 ppm [44]

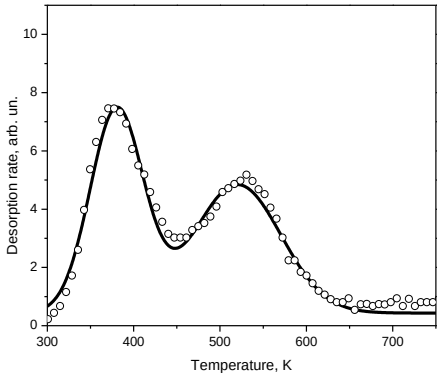

Fig. 3. Experimental points and calculated curve of hydrogen thermal desorption from EI-852 irradiated at T_{room} by H^+ ions to a dose of $2 \cdot 10^{16}$ cm^{-2} [31]

The thermal desorption starts at near room temperature and appears as two peaks in the temperature range between 300 and 750 K [31]. In this work, the depth distribution profiles of deuterium were measured in addition to thermal desorption. The implanted particle depth distribution was measured using the $D(^3He,p)^4He$ nuclear reaction. The measurements were performed at room temperature using forward scattering geometry. 700 and 1000 keV ^3He ions were used to analyze the near-surface region that contained deuterium. The energy spectra of α-particles emitted in the nuclear reaction at different depths at a rate proportional to the local deuterium concentration were obtained.

Using equations (1), the binding energies of deuterium with radiation defects were derived. The calculations were performed under the assumption that 25…30% of the injected gas remains in the material by the end of deuterium irradiation, which is consistent with the data obtained by the nuclear reaction method. It was found that hydrogen is captured by the two types of traps with binding energies of (0.57±0.08) and (0.71±0.1) eV, which corresponds to the gas release stages with maxima at 380 and 520 K (see Fig. 3).

The obtained binding energy value for low-energy traps is in excellent agreement with previous experimental observations [52] and results of recent ab initio calculations for hydrogen trapping by monovacancies in Fe [53]. High-energy traps could be interpreted as vacancy clusters [52] or intrinsic defects associated with precipitates in typical ferritic-martensitic steels, which are considered in detail in Section 1.2.

Tungsten. Currently, tungsten is selected as the main armor material for the plasma-facing components of the next step fusion reactor due to a high melting point, low tritium retention, low sputtering ratio as well as good behavior under neutron irradiation. Meanwhile, it is now believed that fabrication the first wall of a fusion reactor completely from tungsten is not economically feasible due to the high cost, as well as the difficulties with machining due to the hardness and brittleness of tungsten. Recently, tungsten coatings on a stainless steel substrate have come to be considered as an alternative option from the point of view of economics and protection of structural material against plasma exposure [54]. In order to evaluate the applicability of W-coatings as plasma-facing materials, it is necessary to carefully examine the behavior of these materials under irradiation.

Hydrogen isotope retention in various W grades has been studied quite extensively under different experimental conditions. Under low-energy irradiation, vacancies are considered to be the predominant radiation-induced defects. The value of hydrogen de-trapping energy from a single vacancy in W varies among different researchers in the range of 1.3…1.6 eV [55–57].

Recent ab-initio calculations have demonstrated that multiple hydrogen atoms can be trapped around a single defect in W, leading to a distribution of binding energies [57–59]. Furthermore, trapping of multiple hydrogen atoms in one monovacancy is quite possible and the binding energy of subsequent H atoms decreases with increasing occupancy. Following density functional theory calculations [57, 58, 60], hydrogen capturing with de-trapping energy in the range of 1.1…1.2 eV can be attributed to hydrogen multiplicity binding in monovacancies, where it is energetically favorable for up to six hydrogen atoms to participate in the occupancy.

In addition, vacancy clusters have been recognized as extremely strong hydrogen traps in tungsten related materials, which characterized by de-trapping energy in the range of 1.7…2.2 eV [55, 56, 61–63].

In [64], deuterium interaction with tungsten protective coatings deposited by cathodic arc evaporation has been investigated by means of ion irradiation combined with thermal desorption spectroscopy. W samples were treated with 12 keV/D_2^+ ions to a fluence of $(1…10) \cdot 10^{20}$ D_2^+/m^2. Characteristics of experimental TD spectra were associated with specific trapping sites in the material on the base of computational evaluation of

deuterium desorption within the framework of the diffusion-trapping model (1).

Fig. 4 shows deuterium TDS spectra from tungsten coatings irradiated with deuterium ions at temperature 300 K with a fluence of $1 \cdot 10^{21}$ D_2^+/m^2.

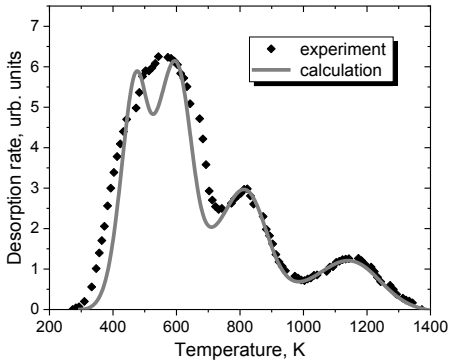

Fig. 4. Experimental points and the calculated curve of thermal desorption of deuterium from W coating irradiated at temperature 300 K by 12 keV D_2^+ ions to a fluence of $1 \cdot 10^{21}$ m^{-2} [64]

The structure of TDS spectra represents the multi-stage process of deuterium release suggesting the trapping of gas atoms by a number of defect types. The derived trapping energy values of 0.94, 1.13, 1.48, and 1.99 eV are associated with deuterium interaction with intrinsic dislocations, radiation-induced monovacancies at multiple and single deuterium occupation, and vacancy clusters, respectively.

Tritium breeder materials. Fusion reactors, which will operate with a closed tritium-deuterium fuel cycle, have a potential to be used for future commercial purposes. However, there are several crucial scientific and technological challenges, which need to be resolved. One of the most important technological challenges for any commercial fusion power plant is to ensure the tritium self-sufficiency. The top priority for tritium breeder materials is the tritium release performance [65]. Understanding of the release behavior of bred tritium from solid breeder materials is necessary to design tritium recovery system from blanket of a fusion reactor because permeation loss of bred tritium in the piping system or type of tritium recovery system depends on the tritium release behavior [66].

Despite the fact that the diffusion of tritium in crystal grains of ceramics is an important step in the process of tritium release, it is also affected by various radiation-induced defects (lithium vacancy, oxygen vacancy, and broken bond). The formation of oxygen vacancies caused by ionizing radiation [67] was found as a possible reason of darkening in the surface of pellets after irradiation. Meanwhile, the lithium vacancy is considered to be the initial defect caused by irradiation in lithium-based materials, since lithium atoms are constantly knocked out from their positions or consumed to form tritium under irradiation [68].

TDS study [69] of ion implanted deuterium in 90% Li_4SiO_4 + 10% Li_2SiO_3 and 90% Li_4SiO_4 + 10% Li_2TiO_3 ceramics indicate that deuterium evolution is observed in the temperature range of 290…650 K and is probably characterized by the superposition of at least two close TDS peaks at around 400 and 500 K. Deuterium gas release from both ceramics demonstrates similar trend indicating weak dependence of deuterium trapping behavior on phase composition.

Performed numerical simulation has revealed that experimental data can be fitted using the following parameters: the activation energy for diffusion E_m = 0.59 eV, the deuterium binding energy with traps Q = 0.40 eV. These values are in reasonable agreement with those predicted by the DFT calculations for Li-based ceramics [70]. Overall, the results indicated that the desorption of deuterium is limited by the intragranular diffusion of deuterium and its trapping by radiation defects associated with Li-vacancy traps.

For the materials considered here, under conditions of the development of low-energy cascades, vacancy type defects appear to be the most preferred trapping sites for hydrogen (deuterium) atoms. The trapping of multiple hydrogen atoms in one monovacancy (up to six as a most common case) is typical for irradiated metals, and the binding energy of subsequent hydrogen atoms decreases with increasing occupancy.

1.2. NANOPRECIPITATE EFFECTS ON HYDROGEN TRAPPING IN STRUCTURAL STEELS

Numerous studies have reported that high strength steels containing large amounts of fine carbide and nitride precipitates have a number of deep trapping sites for hydrogen **[**71–77**]**. Systematical investigation of hydrogen trapping behavior of TiC nanoprecipitates in high-strength martensitic steels by TDS and high-resolution transmission electron microscopy (HRTEM) [74, 75] indicated that the semicoherent TiC nanoprecipitates trap hydrogen at the wide interfaces, while the incoherent TiC nanoprecipitates can trap hydrogen at the internal carbon vacancies during high-temperature tempering. Atom probe tomography (APT) observations [78] allowed to visualize the hydrogen trapping sites by TiC nanoprecipitates. It was recognized that deuterium was enriched at the interface of TiC nanoprecipitates in deuterium filled specimens indicating that hydrogen was trapped at the TiC/matrix interface.

Up to now, hydrogen trapping sites of different metal carbide nanoprecipitates have been investigated extensively. However, there are still open questions regarding the nature of these trapping sites and their effectiveness in immobilizing H.

The interaction between interstitial H and TiC precipitate in Fe has been investigated in [71]. Several types of Fe/TiC interfaces and the interior of the carbide were considered as possible sources of traps for H atoms. In particular, the energetics associated with H trapping for (001)Fe/(001)TiC semicoherent interfaces, (110)Fe/(001)TiC interfaces, C vacancies at these interfaces, and various C vacancy complexes in the interior of the carbides were obtained.

Small TiC nuclei are expected to be fully coherent with the bcc Fe matrix [78]. They are distinguished by a coincidence of atomic planes across the interface, with elastic expansion or compression of one or both phases compensating for any eventual lattice mismatch. With semi-coherent interfaces, the elastic energy required to make the interface coherent becomes prohibitively large.

In order to release the accumulated elastic stress, it is more advantageous to form an array of misfit dislocations. Fig. 5 schematically shows the approximation of a semi-coherent interface by wide coherent regions, which are periodically interrupted by relatively narrow regions containing misfit dislocation cores [79].

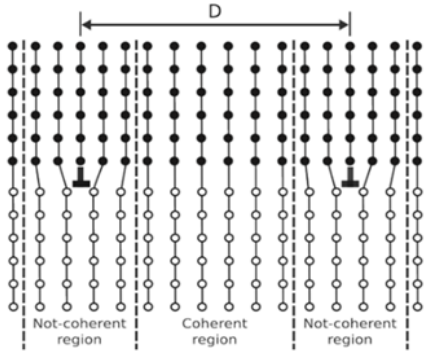

Fig. 5. Schematic representation of the semicoherent interninterface [79]

The coherency of the nanoprecipitates/matrix interface is a key characteristic for the hydrogen trapping capacity that influences the binding energy magnitude of the hydrogen trapping [75, 80]. Fig. 6 shows trap escape energies as function of the source of traps (left) and H desorption energies from various experimental studies as function of the average size of the particles (right).

The binding energy of hydrogen traps at the semicoherent interfaces is slightly higher than grain boundaries and dislocations. A coherent strain field existing near the semicoherent nanoprecipitates in the steel matrix could trap and accumulate a considerable amount of hydrogen in its lattice interstices. Moreover, defects like vacancies and dislocations located at the phase interface, can increase hydrogen absorption ability [81, 82].

The hydrogen trapping sites at the coherent nanoprecipitates interface are at the interfacial tetrahedral gap positions. The binding energy of hydrogen traps at the coherent interface appears to be too low to trap hydrogen effectively, as shown in Fig. 6.

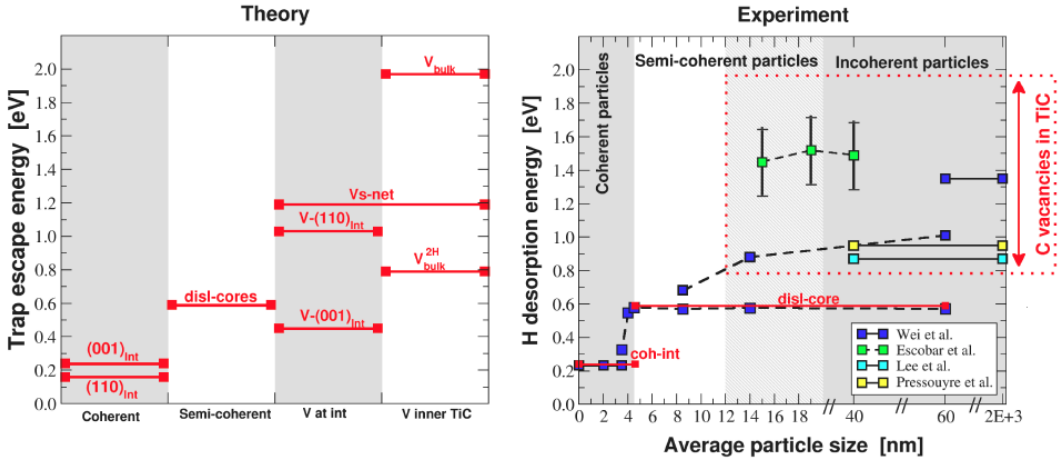

Fig. 6. Left panel: trap escape energies as function of the source of traps. Right panel: H desorption energies from various experimental studies as function of the average size of the particles [71]

The incoherent melal-carbide nanoprecipitates have extremely high hydrogen trap binding energy and their hydrogen trapping sites are associated with internal carbon vacancies [80]. A certain amount of hydrogen can be adsorbed at the incoherent nanoprecipitates interface at low temperatures in some cases [83], but, generally, internal carbon vacancies can trap hydrogen only during the high-temperature heat treatment [75, 80].

For developing structural materials of fusion reactors and core components of advanced fission reactors, ODS-modified steels could be an attractive material because of their corrosion resistance, high-temperature strength and irradiation properties [84]. Recent work suggested that the oxide particles in the ODS steels are effective trapping site for hydrogen and vacancies, so that the oxide particles have an influence on the nucleation and growth of cavities [85]. Depending on coherency conditions, the addition of dispersoid phases in the solid solution can increase significantly the hydrogen uptake due to its trapping at the interfaces of the nanoparticles/matrix. At the same time, hydrogen trapping by the nanoparticles may decrease the hydrogen diffusion to stressed regions preventing the hydrogen embrittlement.

1.3. HYDROGEN TRANSPORT ALONG GRAIN BOUNDARIES

GBs are usually considered as planar defects that affect a variety of properties in polycrystalline metallic materials, including tensile strength, fatigue resistance, thermal and electrical conductivity, corrosion, resistance to hydrogen attack, and others [86–90]. A GB may also serve as a source and sink for vacancies and dislocations because it is a region of partial atomic disorder with definite structure and orientation [91–94].

Concerning the specific role of GBs in H diffusion, there are various and sometimes opposing points of view. Some studies have reported that accelerated H transport along GBs is attributed to low activation barriers and short-circuit diffusion. Meanwhile, there is clear evidence of the inverse observations. The various roles that GBs can play in influencing H diffusion have been demonstrated through comprehensive first-principles calculations and Monte-Carlo simulations [95]. Using symmetric tilt GBs with a [100] tilt axis, the transition

between slow H diffusion and fast H diffusion along the GB was quantitatively demonstrated with a sharp change in the diffusion coefficient H as the GB tilt angle changes.

Low-angle GBs have been shown to contain isolated high barrier regions that trap and suppress H diffusion, while high-angle GBs provide interconnected low-barrier channels that facilitate the transport of hydrogen. The slow-fast diffusion transition caused by dislocation core overlapping has been identified, and the threshold angle at which such a transition occurs has also been predicted. The classical trapping model, in which dislocations are considered as discrete traps, was shown to accurately describe the H diffusivity for low-angle GBs.

In accordance to the Langmuir-McLean segregation isotherm model [96], an analytical view on the hydrogen segregation concentration showed that high excess volume grain boundaries (Σ11-{332} and Σ5-{310}) have high hydrogen segregation densities with various segregation energies. The segregation sites start to be occupied by hydrogen atoms at very low hydrogen bulk concentration, the hydrogen segregation occurs first at the most stable position, the less stable positions start to segregate hydrogen atoms when the first most stable position is close to the saturation (70…80% occupation).

According to extensive atomistic simulations, the segregation energy is essential to the understanding of dynamic processes of solute evolution in materials [97–100]. The minimum segregation energy, commonly used to characterize GB capacity to interact with hydrogen, vary significantly from 0.04 to 0.37 eV depending on the GB character.

Hydrogen-GB interactions and their role in intergranular fracture are well recognized as critical aspects in understanding hydrogen embrittlement in a wide range of typical engineer scenarios. These interactions involve fundamental phenomena like segregation, trapping, and diffusion, which can be explored as a function of grain boundary configuration. In [101], a comprehensive examination of four grain boundaries was performed using the combination of atomistic calculations and experimental data. It was established that elastic deformation has a significant impact on segregation energy, which cannot be simply reduced to a volume change and must take into account the deviatoric component of strain. Furthermore, some major configurations of the segregation energy are dependent on long-range elastic distortion, allowing the elastic contribution to be rationalized in three terms. The antagonistic impact of GBs on hydrogen diffusion and trapping process was explained by analyzing the various energy barriers involved in reaching all of the segregation sites. The segregation energy and migration energy were found to be two critical elements in determining whether the GBs are a trapping sites or a short circuit for diffusion.

1.4. HYDROGEN IN FISSION MODERATORS, CLADDING, AND STRUCTURAL MATERIALS

Taylor's recent review presents [102] a marked role of hydrogen in fission moderators, fuel, cladding, and structural materials.

The neutron transfers the most energy per collision when it collides with an atom whose mass is close to its own. As a result, the best moderators are hydrogen bearing materials. For many years, light- and heavy-water have served as the primary reactor moderators.

Metal hydrides can also be used as hydrogen-based moderators [103]. The thermal stability and sustained operating temperatures of metal hydride moderators represent their most attractive characteristics.

The development of modern microreactors (2…20 MW reactors) is currently quite focused in metal hydride moderators [104, 105]. Microreactors are expected to operate on high assay low enriched uranium (HALEU, 5…20% enrichment). The reactor core requires an effective, high-temperature moderator due to the size and mass restrictions needed to be transportable and the high operating temperatures required to maximize power conversion.

Several options, such as temperature stability, radiation tolerance, heat transfer properties must be considered when choosing a moderator. Yttrium hydride is of particular interest since it has the highest known temperature stability among the metal hydrides [106]. However, even stable hydrides may eventually lose hydrogen at the high temperatures anticipated for microreactors (about 800 °C).

Hydrogen depletion caused by a change in the heat transfer properties of the metal hydride moderator due to swelling or blistering can lead to a decrease in fission output. Therefore, additional efforts are needed to study moderators based on yttrium hydride to ensure their technological readiness.

Zirconium alloys usually used to fabricate fission cladding and structural components are well known for their high corrosion resistance, outstanding mechanical properties, and low neutron absorption. Despite its resistance to high-temperature corrosion, zirconium reacts with high-temperature water to form a ZrO_2 protective layer and free hydrogen.

During its lifetime in a nuclear reactor, corrosion oxide layer grows to a thickness of 100 μm – 17% of the total thickness of the cladding [107]. The native hydrogen concentration in zirconium alloys is on the order of a few wppm. As zirconium absorbs hydrogen from the corrosion reaction, the concentration can increase to several hundred wppm [107], causing deterioration in the mechanical properties of the cladding and structural materials. In addition, it was reported that the corrosion rate of cladding increases in the presence of hydrogen [108]. Hydrogen has also been found to enhance intermetallic diffusion [109]. Enhanced irradiation defect growth has also been attributed to the presence of hydrogen [110–112].

Reduction of hydrogen saturation of zirconium alloys using a modification of the surface due to complex ion-plasma treatment was observed in [113]. The method of nuclear reactions was applied to measure depths-concentration distribution of deuterium in the initial zirconium alloy and alloy coated with CrN, CrAl, and Al_2O_3 after saturation of the gas phase at a temperature of 600...900 K ($P_D = (2…9)\cdot10^{-5}$ mm Hg, period = = 120 min) or by ion implantation.

It is established that when samples are saturated with deuterium from the gas phase, deuterium does not

penetrate into the bulk of coatings, but adsorb in their near-surface regions (Fig. 7).

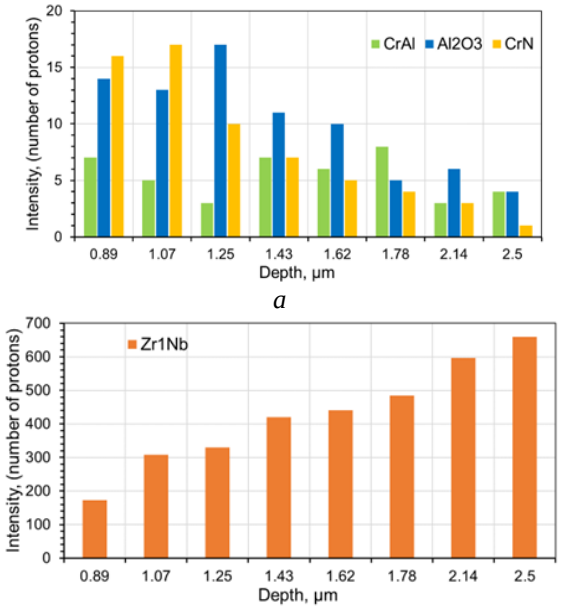

Fig. 7. Depth dependences of integral proton yields for Zr1%Nb samples with (a) and without coatings (b) after saturation with deuterium at a temperature of 720 K [113]

At deuterium implantation in the CrN coating on the Zr1%Nb alloy, its fixation is observed within the ion range, unlike of its redistribution throughout the entire volume of uncoated alloy.

1.5. HYDROGEN EFFECT ON CORROSION AND CRACKING OF STEELS

By interacting with steel during production, processing and operation, hydrogen can be adsorbed on the surface of the metal and subsequently diffuse into the metal lattice. This can result in a decline in mechanical characteristics and early failure of the steel structure. Hydrogen enrichment can not only affect the mechanical properties and microstructure of the metal, but also significantly affect the corrosion behavior of metals. In addition, hydrogen has a strong influence on the composition, structure, electrical properties of passive films and the behavior of steel during pitting corrosion. In order to minimize the negative effects of hydrogen on steel, it is first important to understand the mechanisms by which hydrogen causes deterioration in the performance of steel. Such mechanisms primarily include the following processes:

– Hydrogen can change the composition and structure of the passive film and affect its electrical properties, which ultimately degrades the stability of the passive film. The effectiveness of metal (particularly stainless steel) against corrosion depends significantly on passivation. The thickness of the passive film is about several nanometers, and in the classical model it consists of oxides and hydroxides of Cr and Fe [114]. In the presence of hydrogen, the passivation film changes significantly. It has been established that hydrogen reduces the content of Cr_2O_3 in the passivating film and reduces its thickness [115]. With increasing dissolved hydrogen concentration in a primary circuit of PWR, the Cr content decreases while Fe content increases in the inner layer of the passive film [116]. In addition, an increasing of dissolved hydrogen content in the simulated primary water at 330 °C, leads to a decrease in the thickness of the oxide film and a significant transformation of its structure resulted in overall corrosion rate enhancement [117].

– Hydrogen can enhance the anodic dissolution of metals, affecting the kinetics of oxidation and the kinetics of active dissolution. The influence of hydrogen on anodic dissolution is expressed in the effect of hydrogen on the kinetics of Fe dissolution, as well as the effect of hydrogen on the kinetics of oxidation and the kinetics of film dissolution. Hydrogen can also contribute to a significant increase in the conductivity of the passivating film and additionally contribute to its active dissolution [118].

– Hydrogen affects the electrochemical kinetics of the metal, which subsequently leads to pitting and accelerates the rate of intergranular corrosion. In particular, for welded joints, pitting corrosion can occur at the austenite and ferrite phase boundaries due to the high tendency to enrich with hydrogen at the phase boundaries. In this case, hydrogen can not only enhance the initiation of pitting corrosion, but also affect the microstructure [119].

– The combined action of hydrogen and applied stress can greatly increase the susceptibility of steel to stress corrosion cracking (SCC), especially in welded joints. Several reasons for the influence of hydrogen on SCC are considered [120]. First of all, hydrogen increases the mobility of dislocations, and simultaneously, dislocations facilitate hydrogen transport. These processes contribute to the enhancement of local plasticity and an increase in the dissolution rate. Additionally, hydrogen accumulation at the crack tip facilitates a transition from austenite to martensite. As a result of the galvanic difference, anodic dissolution of the crack tip becomes more intensive, and the SCC threshold decreases contributing to the formation of the SCC expansion path. Lastly, due to hydrogen-associated corrosion, localized corrosion induces the initiation of SCC cracks.

1.6. HYDROGEN INDUCED HARDENING

The phenomenon of irradiation hardening has been widely observed in nuclear structural materials with different crystalline structures. Under high-energy particles irradiation, lattice atoms in the target materials are displaced from their original sites, producing point defects such as interstitials and vacancies that can aggregate to form defect clusters. With plastic deformation, these defects act as obstacles impeding the movement of sliding dislocations, which affect the mechanical behavior of irradiated metals. Generally, the hardness of irradiated materials tends to increase with the irradiation dose until the density of irradiation-induced defects reaches saturation. The formation and growth of radiation defects is a complex process that is determined by material properties and irradiation conditions, including irradiation temperature, irradiation dose, flux, etc. [121].

Of particular interest is the effect of irradiation with hydrogen ions on hardening behavior in structural

materials. In study [122], nanoindentation and Laue microdiffraction were used to characterize both the mechanical response and microstructure evolution in 304 SS due to irradiation. The irradiations were conducted using 2 MeV protons. Specimens of 304 SS were irradiated to 1 and 10 dpa with a dose rate of ~ $8 \cdot 10^{-6}$ dpa/s at 360 °C. It was found that the 1 dpa sample hardness profile is correlated with the calculated dpa profile with less hardness at the near surface area and higher hardness at the end of the stopping region. In contrast, the hardness at the 10 dpa sample plateaus over the entire radiation damaged region. This indicates that after a dose of 10 dpa it is impossible to detect further hardening that suggests saturation of the material with radiation defects. The saturation effect is not unique to H irradiation, but has been observed in other studies [4, 123]. Comparing the nanoindentation data with FWHM (Full Width at Half Maximum) from Laue microdiffraction it was suggested that a linear correlation between these two parameters may exist considering that FWHM and nanoindentation are based on the dislocation density.

The effect of hydrogen on mechanical properties (hardness and elastic modulus) and microstructure has been investigated in Fe-10Cr alloy as a reduced-activation ferritic/martensitic steel model following ion irradiation with 100 keV H ions to a dose of $7 \cdot 10^{16}$ H^+/cm^{-2} at 773 K [124]. Nano-indentation results showed that pronounced irradiation hardening was induced by H irradiation. Nanohardness of H^+-irradiated sample was increased to 3.87 GPa as compared to 2.35 GPa in the non-irradiated sample. A large number of dislocation loops have been observed in the steel after ion-irradiation relative to the non-irradiated material. The density of the dislocation loops was accounted to be $5.1 \cdot 10^{21}$ m^{-3}, and their average size was ~ 8 nm after H ion irradiation. The mechanism of hardening could be strongly associated with dislocation loops formation. Modulus was not found to have noticeable changes.

Somewhat surprising results were obtained when studying the effect of hydrogen charging on the plastic deformation of nanocrystalline nickel [125]. The influence of hydrogen was analyzed by means of nanoindentation on the uncharged and hydrogen-charged samples. It was revealed from TDS analysis that the H mainly resides in fcc lattice, GBs and vacancies rather than dislocations. Nanoindentation tests indicated that H charging significantly reduces the hardness and enhances the pile-up around indentation. This H-induced softening behavior was explained by H-enhanced activity of partial dislocations emitted from GBs and/or abundant H-vacancy cluster formation around GBs.

Although mechanisms for the phenomena of irradiation hardening are fairly well documented, and a consensus has been reached that the irradiation-hardening mainly originates from the impediment of sliding dislocation by irradiation-induced defects, additional efforts are needed in the field of hydrogen effects on the formation of irradiation-induced defects, dislocation-defect interaction, and evolution of defects and dislocations.

2. HELIUM

2.1. NUCLEATION AND GROWTH OF He BUBBLES

Beyond radiation induced defects, high-energy nuclear transmutation reactions produce large quantities of helium atoms in materials. Since helium exhibits an extremely low solubility in metals, it tends to agglomerate into nanosized He bubbles in structural materials [126–129]. Typical examples of transmission electron microscopy (TEM) micrographs of He bubbles in W [130] and Ni [131] formed after He^+ ion irradiation are shown in Fig. 8.

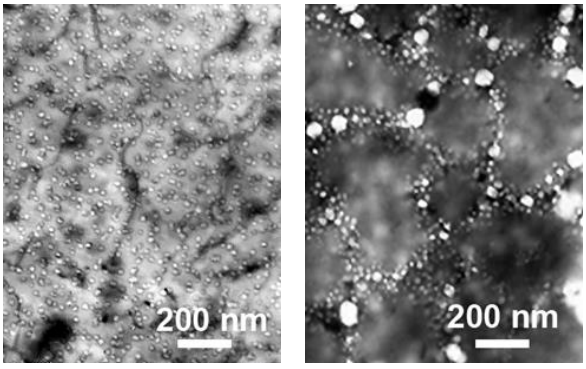

a *b*

Fig. 8. TEM micrograph of nearly uniform He bubbles distribution in W [130] (a) and segregation of He bubbles at grain boundaries in Ni [131] (b)

A comprehensive understanding of the role of bubbles in metals requires a detailed evaluation of bubble formation mechanisms, including the stages of nucleation, growth, and coarsening of bubbles. All these stages are associated with intense interaction of point defects (vacancies and interstices) with He atoms and are controlled by diffusion, dissociation and clustering processes. At the early stage of bubble nucleation, the limited spatial resolution of available experimental techniques hinders the direct in-situ observation of bubble formation and prevents the detection of the mechanisms underlying bubble nucleation. Therefore, studies on this issue are usually carried out using computer simulation methods [132–140].

Significant efforts in this regard have been focused predominantly on bcc iron and tungsten as main components of nuclear reactor and plasma facing materials. Using first-principles methods, several studies [141–143] pointed out that interstitial He is energetically favorable to occupy the tetrahedral interstitial site (TIS) with low formation energy in bcc metals. For instance, ab initial calculations [142] indicate that the formation energies of interstitial He in tungsten at TIS is 6.18 eV, which is slightly lower than that in octahedral interstitial sites (6.40 eV). Similar trend that TISs are preferable He traps was confirmed in other studies [143, 144].

Interstitial He atoms are characterized by low migration energy in metals and easy trapping by vacancies due to their high binding energy [134, 145]. In addition, the interstitial helium atoms are mutually attracted to each other, and, as a consequence, the He atoms are more likely to self-trapping and aggregate due to the strong attraction, thereby forming clusters [146].

Further, the interstitial noble gas clusters and vacancy-noble gas atoms complexes have been demonstrated to energetically prefers to grow through trapping additional isolated noble gas atoms, because of the strong self-trapping between themselves, thereby giving rise to He bubble nucleation in metals [147–151]. Fig. 9 schematically illustrates tendencies for a He atom binding to a He_xV cluster and a He_x cluster, according to data [148, 150, 151]. The binding energy of an additional He atom to a He_xV cluster initially decreases and then remains almost constant at a value of about 1.3 eV with further increasing He atoms. The binding energy of an interstitial He to an interstitial He cluster generally increases with increasing cluster size, and approaches a value of about 1.4 eV when the total number of He atoms is larger than eight.

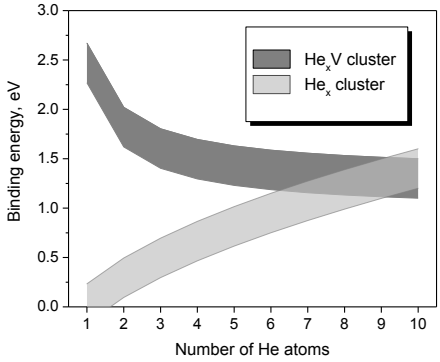

Fig. 9. Binding energy of an additional He atom to a He–V cluster and to a He cluster

If the interstitial He cluster is sufficiently large, it can create a Frenkel pair. The corresponding vacancy is incorporated into the existing He cluster, and the resulting helium–vacancy cluster becomes immobile [150]. Subsequent accumulation of He in He–V clusters will contribute to the significant increase of the pressure created by He–V clusters on surrounding lattice. As a result, the matrix atoms surrounding He–V clusters will be kicked-out due to the high pressure, producing Frenkel pairs. The kick-out mechanism creates additional vacancies and interstitials, lowering He/V ratio in He–V clusters. The binding energy of helium atoms to He–V clusters with low He/V ratio is rather high [152]. This implies that He–V clusters with low He/V ratio are strong sinks for He atoms, and thus the kick-out mechanism significantly enhances He bubble nucleation and growth.

In addition to the kick-out of individual matrix atoms, the growth of over-pressurized bubbles is provided also by multiple interstitials pushing altogether which rearrange into a prismatic dislocation loop [153–155] or single dislocations which evolve into a prismatic dislocation loop [156]. It was demonstrated, that SIAs pushed out by high pressure He bubbles can form crowdion structure around He bubbles [134–137, 140]. In bcc metals the crowdion structure usually exhibits an energetically favorable orientation along <111> direction [132, 134, 140, 145]. With further increasing He concentration, SIAs continuously accumulate around He bubbles, leading to the formation and emission of dislocation loops. This well-known helium bubble growth mechanism, named as dislocation loop punching. Alternative loop-punching mechanism for He bubble with larger initial radius was proposed in the case of tungsten. It was shown, that a large-size bubble grows by pushing out a dislocation, subsequently cross-slipping of its screw components and finally evolving into a prismatic dislocation loop. With the accumulation of the dislocation, a dislocation network can form around the He bubble [156].

The punched out entities are emitted from the bubble, releasing the high local strain caused by bubble growth. Dislocation loop punching can only be triggered above certain critical He pressure. Some theoretical approaches were proposed in order to identify the punching criteria [157, 158].

When subjected to thermal annealing at a high temperature, noble gas bubbles will tend to undergo coarsening – a thermodynamically favorable process in which the average bubble size increases at the expense of reduced bubble number density. Generally, two different mechanisms, migration and coalescence (MC) and Ostwald ripening (OR), have been proposed for bubble coarsening under annealing [159–164]. MC mechanism mainly depends on the rearrangement of bubble surface through diffusion of internal surface atom [161, 162]. In this case, the activation energy of processes leading to a change in the bubble density during annealing is about half the surface diffusion energy, which depends on the thermodynamic state of the bubbles. OR mechanism is driven by different equilibrium pressure of bubbles with different sizes [163, 164]. This process is due to thermally activated dissociation of vacancies and gas atoms from small bubbles and their re-absorption by larger bubbles, which leads to the shrinkage of small bubbles and growth of larger ones. In the case of OR, the apparent activation energy for reducing the bubbles density is equal to the helium dissociation energy from the bubbles, which is much higher than surface diffusion energy. It is believed, that the MC and OR mechanisms will dominate at relatively low and high temperatures (and/or high and low helium concentrations), respectively. In addition to the dissociation and reabsorption of helium atoms, the OR mechanism requires the dissociation and reabsorption of vacancies. Thus, this mainly two-component mechanism can be controlled by the process of dissociation of He atoms or vacancies, depending on which of the two dissociation energies is higher.

Helium bubbles growth by MC mechanism was experimentally demonstrated in [165]. In these in situ experiments, samples of Fe-16Cr-17Ni alloy were irradiated with 10 keV helium ions using an ion accelerator connected to an electron microscope. Some samples irradiated with He^+ ions were annealed to temperatures of 970…1500 K, and the movement of bubbles was continuously monitored and recorded on video. It was found that bubble nucleation dominates at 700 K, while bubble growth processes dominate at temperatures above 900 K. The mobility of helium-vacancy complexes or bubbles was found to be an important factor regulating these processes. The diffusivity of helium bubble depends on its diameter and was estimated as 10^{-18}…10^{-20} m^2/s at 1460 K. During the Brownian motion, the bubbles coalesced and disappeared on the surface of the sample.

The in-situ TEM observation [166] of thermally activated processes occurring in Ni films irradiated with He^+ ions revealed both mechanisms of bubble growth. It was shown that immediately after the bubble's formation, their growth occurs due to the diffusion of helium atoms or helium-vacancy complexes of varying complexity. With increasing of temperature up to ~ 800 K, along with diffusion growth, the process of bubbles coalescence was detected. The time of single coalescence event ranges from 0.04 to 0.25 s. With a further increase in temperature, this process became more evident, and at irradiation dose of $2 \cdot 10^{21}$ m^{-2}, leads to the formation of extended gas-filled cavities. Simultaneously with the bubbles growth, annihilation processes were also observed: a decrease in the bubble diameter up to their complete disappearance (Fig. 10). In addition, processes of growth of a large gas-filled cavity occur due to the gas atoms flow from a nearby small bubble.

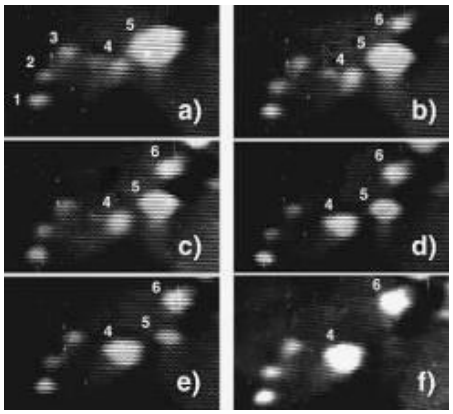

Fig. 10. A series of micrographs illustrating the growth of bubble 4 by combining with smaller surrounding bubbles, disappearance of bubble 5 and synchronous growth of bubble 6. Bubble 1, 2, 3 do not change [166]

Each of the bubble growth mechanisms is associated with a certain trend in the dependence of bubble sizes and densities on the annealing temperature. Fig. 11 shows the temperature dependences of the average diameter and density of helium bubbles for a dose of $1 \cdot 10^{21}$ m^{-2}.

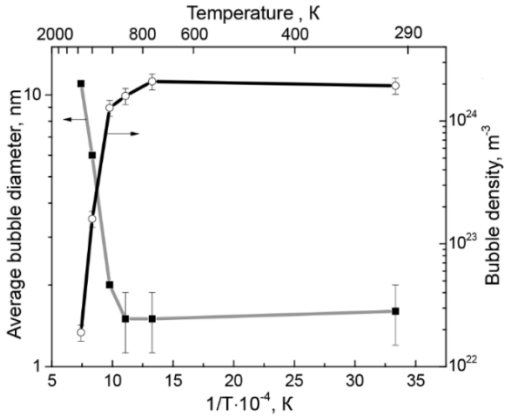

Fig. 11. Temperature dependence of the average size and density of helium bubbles in 18Cr10NiTi steel irradiated with 20 keV helium ions to a dose of $1 \cdot 10^{21}$ m^{-2} [167]

The experimental data are characterized by three temperature intervals: 1 – from 300 to 760 K; 2 – from 760 to 1030 K, and 3 – from 1030 to 1350 K with clearly different trends.

In the low-temperature region, the diameter and density of the bubbles remain virtually unchanged. Upon annealing in the temperature range 760…1030 K, their sizes begin to grow and the density slightly decreases. This trend is significantly enhanced in the temperature range of 1030…1350 K. An assessment of the activation energy (the slope of the high-temperature branch of the curve) of the last process, associated with pronounced enlargement of helium bubbles has produced a value of ~ 3.7 eV, which agrees well with the theoretically calculated activation energy (3.5 eV) of the process of detachment of a helium atom from a microbubble according to the OR mechanism [168].

Several studies indicate that the composition and microstructure of material significantly affect bubble coarsening mechanism. For instance, bubble migration and coalescence in He-irradiated high purity Fe under annealing at 750 °C were more intense as compared to Fe-9Cr alloy [169]. These results suggest trapping effects of vacancies by Cr and its influence on the bubble formation. Further, TEM characterization of microstructure evolution in 20Cr-40Fe-20Mn-20Ni high entropy alloy (HEA) and 18Cr10NiTi steel after He-irradiation and subsequent annealing at 500 °C reveals that He bubbles in 18Cr10NiTi steel and Cr-Fe-Ni-Mn alloy exhibit different morphology and density [170]. In the case of steel, very small and sparse spherical helium bubbles with an average diameter of ~ 1.6 nm and a density of $1.0 \cdot 10^{24}$ m^{-3} have been observed. In contrast, numerous bubbles with average diameter of ≤ 1.0 nm were detected in irradiated Cr-Fe-Ni-Mn alloy. The suppression of bubble formation can be related to the HEAs' intrinsic properties, i.e. severe large lattice distortion and chemical disorder which reduces helium diffusivity in Cr-Fe-Ni-Mn that results in suppression of helium bubbles nucleation and growth. In addition, post-irradiation annealing of He-irradiated RAFM steels with and without ODS additions showed the formation of large helium bubbles in ODS-steel, while high-density small He bubbles were observed in conventional alloy [171]. It was anticipated that different He bubble behavior in these two materials depends completely on the microstructure.

2.2. He AND H SYNERGISTIC EFFECTS ON RADIATION HARDENING AND SWELLING

The irradiation damage significantly depends on the neutron energy spectrum, temperature, irradiation dose, and dose rate. The displacement cascades produce a variety of defects, but of particular concern is the simultaneous production of helium and hydrogen and their effects in structural materials. For iron-based materials, the typical production rate of helium and hydrogen is estimated as ~ 1 appm/dpa in fission reactors, ~ 10 appm He/dpa and ~ 40 appm H/dpa in fusion reactors, and up to 100 appm He/dpa and 500 appm H/dpa in spallation facilities [172]. The experimental data collected over the last few decades indicate that the He–H synergistic effects strongly influence the evolution of damaged microstructures, causing deterioration in the performance of structural

materials, such as swelling and radiation hardening. Moreover, the effects associated with damage/helium/hydrogen synergy can significantly exceed the effects caused by displacement defects alone [173].

To date, the overall majority of performed studies on He–H synergistic effects were based on multi-ion beam irradiation. Multiple simultaneous ion beam irradiation, i.e., Heavy Ions + He + H, has served as a convenient tool for the simulation of these phenomena over a variety of temperature and dose regimes due to the ability to widely vary and control the irradiation parameters, such as temperature, dose, dose rate, He and H production rate.

In recent decades, a number of studies [174–190] have been carried out within the framework of synergistic effects between radiation damage and transmutation gas production, but their results are not always consistent. The increase in swelling due to He–H synergistic effects had been demonstrated in the earliest investigations conducted by Farrell and Lee [174] using dual beam (Fe + He) and triple beam (Fe + He + D) irradiation of Fe10.5Cr6Mo ferritic/martensitic steel to 100 dpa and a gas co-implantation level of 40 appm D/dpa and 10 appm He/dpa at 500 °C. More than a tenfold increase in swelling (~ 3.2% vs ~ 0.08%) was reported in F82H irradiated to 50 dpa with the co-injection of hydrogen and helium at 70/18 appm/dpa of H/He at 470 °C [175–178]. The same tendency was observed in other materials under different experimental conditions [179–184]. On the contrary, results of study [185] indicate that the cavity swelling of pure alpha Cr was 0.8% under single beam irradiation, while a notably lower swelling of 0.5% was registered under triple beam irradiation. In addition, some results [186–188] showed that the swelling can be enhanced or suppressed under different multi-beam irradiation regimes, indicating that He–H synergistic effects on swelling appear to be ambiguous.

Most studies demonstrate that the simultaneous injection of helium and hydrogen results in increasing of cavity number density, suggesting that the He–H synergistic effects facilitate cavity nucleation. Meanwhile, the synergy effects on the change of cavity size is not so obvious. For instance, the largest bubbles were found within the depth range of superposition of maximum displacement damage and highest gas concentration after triple beam (Fe + He + H) irradiation of EUROFER97 at different temperatures [189]. This observation suggests that synergistic effects between helium and hydrogen should strongly promote bubble growth. Alternative results were obtained in the case of pure Fe irradiated with (Fe + He + H) simultaneous ion beams [190], where the largest cavities were found in the area with high level displacement damage, but neglectable concentration of co-implanted H/He gaseous atoms.

Advances in understanding the complicated synergistic effects on cavity swelling can be achieved by considering the contribution of individual components, i.e. helium and hydrogen, separately. The role of helium alone in the nucleation of high densities of bubbles at a wide range of damage levels and its effect on the development of cavity microstructures in irradiated structural materials is well described in general terms [186,191–194]. The simultaneous co-injection of helium with displacement damage leads to significant increasing of the number density and size of cavities compared to damage alone, thereby enhancing swelling [159, 195].

Several studies [191, 196, 197] have shown that at a low helium concentration, the cavity swelling initially increases with increasing He concentration. As helium content increases from moderate to high, small pressurized bubbles and relatively large underpressurized voids can lead to a bimodal cavity size distribution. At extremely high helium concentration, the size distribution of the cavities again becomes monomodal, which is associated with a high density of helium bubbles.

It was recognized that the irradiation swelling strongly depends on the He implantation ratio (appm/dpa). According to [198], this dependence has a pronounced non-monotonic character in austenitic steels and several other fcc metals. Fig. 12 demonstrates the effect of He/dpa on cavity swelling in pure Cu irradiated between ~ 1…10 dpa.

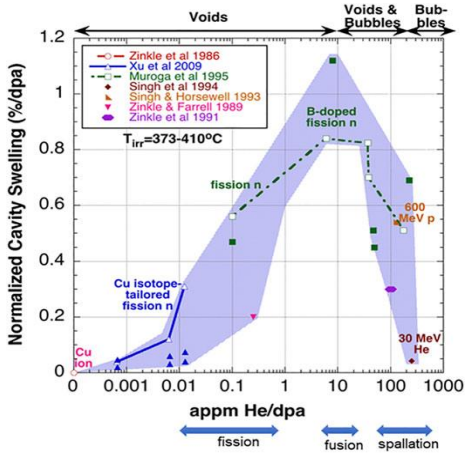

Fig. 12. The cavity swelling in pure Cu versus the production rate of He [198]

This non-monotonic behavior of cavity swelling was interpreted in the framework of concepts based on the variation of the sink strength ratio [192]: the initial increase in cavity swelling can be attributed to early nucleation induced by He, which increases as long as the dislocation and cavity sink strengths are equal. The cavity swelling peaks at intermediate level of about 10 appm He/dpa. After that, as the helium implantation continues to increase, the intense nucleation leads to the higher cavity densities and predominance of cavities as a sink, and hence, swelling tends to decrease by slowing down the growth rate of the cavity.

Hydrogen is believed to play a secondary role as compared to helium because of its high mobility and easy desorption from steels. Contrary to helium, hydrogen's function has not been conclusively determined, which may be the primary cause of the variance in the He–H synergistic effects.

Early studies on vanadium alloys [180] and Fe-Cr ferritic alloys [181] indicate that H has a limited effect on cavity evolution when interacting with point defects alone, because the cavity size, density, and swelling remained largely unchanged under dual (Heavy Ion + H) beam irradiation compared to single self-ion irradiation.

On the other hand, the addition of H to the triple beam irradiation (Heavy Ion + He + H) resulted in a considerable increase in cavity size, a decrease in density, and an enhancement of swelling as compared to (Heavy Ion + He) dual beam, thereby indicating that H may efficiently stimulate cavity growth. The contrasting roles of hydrogen in these two scenarios suggested that H may have an impact, especially in the synergistic effects between He, H, and vacancies.

A more recent study [188] on 8…12% Cr ferritic/martensitic steels analyzed the effects of hydrogen/helium through a wide range of gas injection levels. It was found that contrary to single self-ion irradiation, the presence of H in the dual-ion beam (Cr + H) irradiation caused a noticeable reduction in cavity average size. At the same time, the density was increased by approximately 100 times. With increasing implanted hydrogen content, the cavity size tended to decrease, while the density increased continually.

In most recent study [185] dual and triple ion beam irradiations were performed on alpha-Cr using Fe^{++}, He^{++}, and H^{+} ions in order to examine the synergy of hydrogen and helium on cavity formation. Results indicated that the co-implantation of hydrogen with iron leads to a significant cavity growth. In addition, the size and density of cavities under (Fe + H + He) triple beam irradiation increased compared to (Fe + He) dual beam, indicating that H facilitate the nucleation and growth of cavities in synergistic effects. It was noted, that under triple beam irradiation, hydrogen can accelerate cavity nucleation via stabilizing initial embryos.

The individual role of hydrogen and helium atoms in the synergistic effect was studied by helium and hydrogen single-beam (He or H) and sequential-beam (He/H or H/He) irradiation of reduced-activation martensitic steels [199]. Swelling was found to increase considerably following sequential-beam irradiation compared to single-beam irradiation. In addition, the size of cavities and swelling was smaller under sequential H/He irradiation compared to sequential He/H irradiation. It was speculated that such observations can be regarded to the decomposition of H–V clusters at H/He irradiation regime, while under sequential He/H irradiation, the post-implanted H could be trapped by relatively stable He-V clusters, resulting in the increase of H concentration in the clusters. The specific roles of hydrogen atoms in the synergistic effect include assisting in the nucleation of helium bubbles, enhancing helium atom diffusion, and helping in the growth of helium bubbles. The probable roles of helium atoms are the formation of the initial helium bubbles and enhancing the retention of hydrogen atoms to form He–H-vacancy complexes. Thus, the simultaneous interaction of helium, hydrogen and radiation damage promotes gas bubble formation and leads to an increase in swelling.

Under triple beam simultaneous irradiation, the stable He–V clusters can also trap hydrogen atoms to form He–H-vacancy clusters and dominate the evolution of cavities [200]. He–H-vacancy clusters formed in He–H synergistic effects are believed to be more stable compared to H–V clusters, from which H could dissociate and escape under certain irradiation conditions. The research results also indicate that hydrogen does not accelerate cavity growth at temperatures below the maximum swelling temperature, but contribute to the stability of He–V clusters. However, at higher temperatures, the extremely high diffusivity of hydrogen atoms would hinder their interaction with the developing He–V clusters [173].

Unlike to the fairly large amount of data on swelling behavior, very limited information was reported on the mechanical properties evolution caused by synergistic effects of helium and hydrogen in structural materials. Among the earliest, these effects were studied by means of nanoindentation measurements conducted on type 316LN stainless steel which was implanted with Fe, He, and H ions, alone and in combination [201]. Helium-induced hardening was found to be twice the level measured for iron-induced displacement damage alone. The additional hardening resulted in helium injection was associated with the presence of helium bubbles. It was also observed that co-injection of He and H caused more hardening compared to He-implantation alone, as shown in Fig. 13.

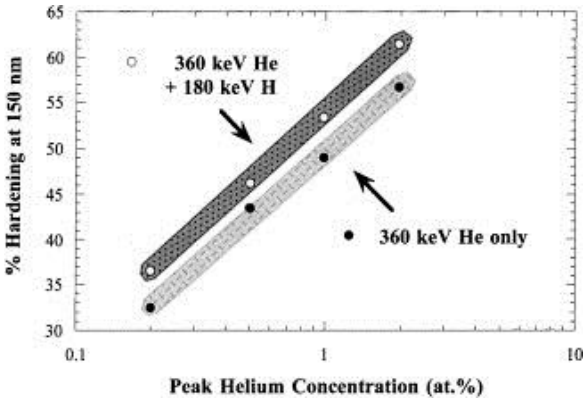

Fig. 13. The dependence of irradiation induced hardening on He-concentration for 316LN stainless steel implanted with He only (solid circles) and those co-implanted with an additional amount of H (open circles) [201]

Performed observations suggest that under irradiation conditions that include both helium and hydrogen, hydrogen trapping by helium clusters may enhance the irradiation hardening effect caused by gas bubbles.

Another study on F82H ferritic/martensitic steel also indicate that H has a synergistic effect on mechanical properties under triple beam irradiation conditions as compared to single beam (Fe) and dual beams (Fe + He) [177]. It was shown that the presence of He or He + H in the 270 °C irradiations has negligible effect on the microhardness, while measurable increase in the microhardness was registered at 360 °C for the dual and the triple beam irradiations compared to the single beam irradiation (Fig. 14).

It was noticed that no helium filled cavities were found under double-beam irradiation at 270 °C, while they were observed at 360 °C. Therefore, hydrogen appears to have a synergistic effect only when helium clusters or bubbles are available with which hydrogen can interact [177].

Lastly, synergistic effects of H and He on the mechanical properties of Fe-10Cr ferritic/martensitic steel were investigated in recent study [202] using

sequential and separate irradiation of steel specimens with H and He ions. The indentation stress-strain tests were performed by nanoindentation after the ion irradiation. The authors reported that the sequential irradiation by He and H resulted in a higher indentation yield stress than separate irradiation, suggesting that the hardening was enhanced by the synergy of the hydrogen and helium irradiation.

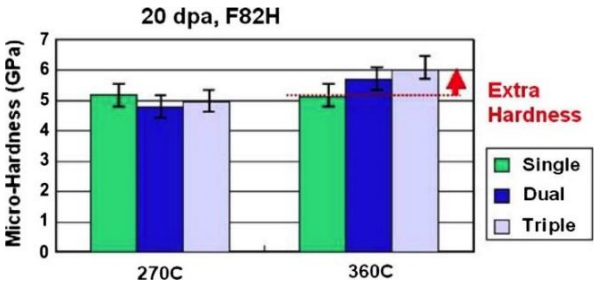

Fig. 14. Microhardness of F82H steel irradiated to 20 dpa at 270 and 360 °C for three beam conditions, single, dual and triple [177]

As expressed above, discussed data suggest that under irradiation conditions involving the production of transmutation gases (He and H), an increase in radiation hardening should be expected due to the synergy of displacement damage, helium and hydrogen. However, the limited amount of data indicates the need for additional experiments.

2.3. HELIUM BUBBLE-HYDROGEN INTERACTIONS IN METALS

Due to the inconsistent results observed in swelling studies employing simultaneous multi-beam irradiation, interpretations for the effect of hydrogen on these processes vary considerably. It has been suggested that the effect of hydrogen is often manifested in enhancing helium atom diffusion, assisting in the nucleation of helium bubbles, and helping in their growth.

An early evidence of hydrogen effect on helium-filled cavities formation was proposed in study on simultaneous (double- and triple-beam) irradiations of ferritic steel [179] followed by TEM analysis of bubbles distribution in material. It was observed that the presence of deuterium increases the nucleation of helium bubbles compared to double-beam irradiation, decreasing bubble size but increasing bubble density. The authors suggested that hydrogen could facilitate helium bubble nucleation by reducing the surface energy. According to the critical bubble model [203], the critical bubble size is proportional to the surface energy, hence the reduction in surface energy will lead to a decrease in the critical bubble size. In other words, the enrichment of the bubble interface with hydrogen atoms could significantly influence bubble formation and swelling.

Two basic mechanisms for hydrogen trapping at helium bubble interfaces have been suggested: a chemisorption-like trapping mechanism [204], and a stress/strain field mechanism [205]. The first option assumes that hydrogen undergoes a chemisorption-like interaction at the inner walls of helium bubbles with a binding enthalpy close to that for chemisorption. For instance, de-trapping experiments on D in He-implanted Fe gives a de-trapping enthalpy of 0.75 eV [206], which is correlated with calculated energy for chemisorption of H on an internal free iron surface of 0.73 eV [207]. The second case represents the trapping of hydrogen close to the bubble-matrix interface. According to this model, hydrogen atoms are attracted toward the outer bubbles surface due to positive stresses created by high pressure inside the bubbles. Calculated trapping energy between H atoms, and helium bubbles has been derived to be 0.71 eV [205]. Furthermore, in recent paper [208] the conjunction of both hydrogen attraction to strain fields mechanism and chemisorption-like mechanism has been suggested. This model assumed, that the strain fields may attract and accumulate the solute hydrogen around the bubbles, some fraction of which subsequently passes in a chemisorbed state. Fig. 15 shows a schematic localization of H atoms within 2 nm bubble. Hydrogen is both on the surface of the bubble and inside the first layers of metal matrix.

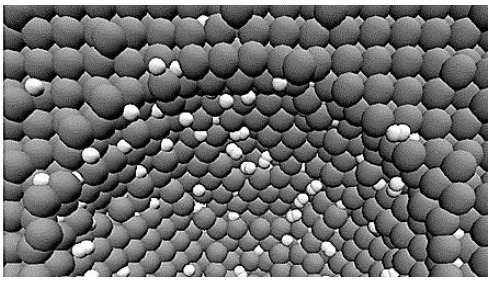

Fig. 15. Schematic representation of hydrogen distribution at the bubble interface. The dark gray and light gray balls are W and H atoms, respectively [209]

It is worth noting, that considered mechanism of hydrogen interaction with cavities was observed not only for helium-filled cavities. Similar behavior has also been recognized in the case of argon-filled cavities in 316 SS [210]. Moreover, the trapping energy between H atoms, and Ar bubbles was estimated as 0.74 eV, i.e. virtually coincided with above He-associated case.

Fundamentally different mechanism of hydrogen retention was proposed for the interpretation of unexpectedly high levels of retained hydrogen in stainless steels irradiated in a PWR, FFTF, and HFIR [211]. For instance, up to 3800 appm of hydrogen was detected at analyzing baffle-former bolt fabricated from cold-worked Type 316 SS after exposure to a fluence of 7.5…12.5 dpa at 606…616 K. Although hydrogen retention was attributed to the presence of cavities, it was suggested that such large hydrogen quantities cannot be in atomic form and trapped close to cavity surface. The hypothesis was that hydrogen is stored in cavities as H_2 molecular gas.

Recently, severe efforts have been made to identify the mechanism of H_2 formation within the nanocavity in the metal matrix [212]. It turned out that this process is highly dependent on hydrogen concentration. Density functional theory calculations for the H–Fe system [213] have showed that at low hydrogen content, hydrogen atoms coat the surface of the cavity and interact primarily with nearby iron atoms. As more hydrogen is introduced into the cavity, and the surface saturates with hydrogen, the formation of H_2 molecules becomes possible in the center of the cavity. When both hydrogen and helium are present within the vacancy cluster [214], atomistic

simulations predict the formation of a core of helium that is surrounded by a shell of hydrogen atoms which are attracted to the bubble's free surface.

Several experimental studies [189, 215, 216] supported above simulation results and confirmed the existence of He and H within a cavity by means of EELS. Fig. 16 shows an example of the elemental maps for two adjoined cavities in triple ion irradiated RAFM steel [215]. These data indicate that helium has formed a core-like structure in the center of cavity, while hydrogen appears to be present at cavity periphery, forming a shell or halo.

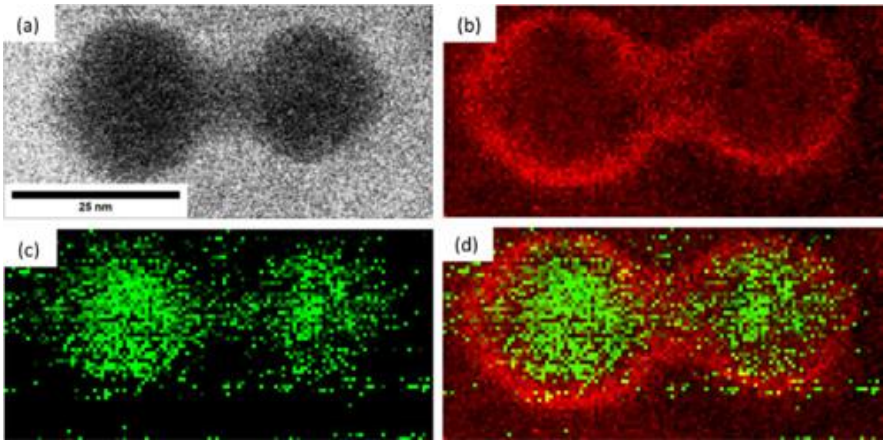

Fig. 16. STEM-HAADF image of cavities in triple ion irradiated Fe8Cr2W steel (a), EELS spectral map integrated for the H-K peak (b), He-K peak (c) and composite of H-K and He-K EELS spectral maps (d) [215]

It should also be pointed out, that experimental confirmation of H_2 formation within the cavity is extremely rare. At least to our knowledge, only one H_2 observation was reported for Fe-based alloys. SIMS analysis of Fe-12 wt.%. Cr-ODS steel irradiated with single, double and triple beams showed the presence of a peak corresponding to H_2 in the Raman spectra [217]. Remarkably, that molecular hydrogen was detected only in experiments with the simultaneous presence of hydrogen and helium.

SUMMARY

This paper has reviewed some issues of hydrogen and helium interaction with structural materials for nuclear applications. The individual features of He and H trapping behavior in various materials were considered, and their synergistic effects in terms of radiation hardening and swelling were analyzed. Progress in developing experimental and computational techniques has enabled researchers to better study the characteristics of gas-metal interactions. Although many mechanisms have been proposed for explaining the effects of transmutant gases on the structure and properties of materials, additional efforts are needed for comprehensive understanding of the phenomena of hydrogen- and helium-induced degradation of reactor materials. This issue is most critical for the structural materials of advanced nuclear reactor systems due to the increase of the core outlet temperature and high dose of the core internal structures of the new reactor systems.

ACKNOWLEDGEMENTS

The work was financially supported by the National Academy of Science of Ukraine (program "Fundamental scientific research on the most important problems of the development of scientific and technical, socio-economic, socio-political, human potential to ensure Ukraine's competitiveness in the world and sustainable development of society and the state").

REFERENCES

1. В.Н. Воеводин, И.М. Неклюдов. *Эволюция структурно-фазового состояния и радиационная стойкость конструкционных материалов*. К.: «Наукова думка», 2006, 374 с.

2. S.A. Karpov, G.D. Tolstolutskaya, V.N. Voyevodin. The most probable mechanisms of material characteristics degradation due to accumulation of hydrogen and predicting the possible scenarios of maintain its resource // *PAST*. 2018, N 5(117), p. 3-15.

3. H. Zhang, C. Zhang, Y. Yang, Y. Meng, J. Jang, A. Kimura. Irradiation hardening of ODS ferritic steels under helium implantation and heavy-ion irradiation // *J. Nucl. Mater*. 2014, v. 455, p. 349–353.

4. Gary S. Was. *Fundamentals of Radiation Materials Science: Metals and Alloys.* Springer, 2016, 1002 p.

5. J. Hure, A. Courcelle, I. Turque. A micro-mechanical analysis of swelling-induced embrittlement in neutron-irradiated austenitic stainless steels // *J. Nucl. Mater*. 2022, v. 565, p. 153732.

6. *Gaseous hydrogen embrittlement of materials in energy technologies. V. 2: Mechanisms, modelling and future developments* / Edited by Richard P. Gangloff and Brian P. Somerday. Woodhead Publishing Limited, 2012, 500 p.

7. И.М. Неклюдов, Г.Д. Толстолуцкая. Гелий и водород в конструкционных материалах // *Вопросы атомной науки и техники. Серия «Физика радиационных повреждений и радиационное материаловедение»*. 2003, №3, с. 3-14.

8. J. Venezuela, Q. Liu, M. Zhang, Q. Zhou, A. Atrens. A review of hydrogen embrittlement of martensitic advanced high-strength steels // *Corros. Rev*. 2014, N 34, p. 153-186.

9. Y. Hagihara, T. Shobu, N. Hisamori, H. Suzuki, K. Takai, K. Hirai. Delayed Fracture Using CSRT and Hydrogen Trapping Characteristics of V-bearing High-strength Steel // *ISIJ Int*. 2012, v. 52(2), p. 298-306.

10. G.D. Tolstolutskaya, V.V. Ruzhytskiy, I.E. Kopanetz, S.A. Karpov, V.V. Bryk, V.N. Voyevodin, F.A. Garner. Displacement and helium-induced enhancement of hydrogen and deuterium retention in ion-irradiated 18Cr10NiTi stainless steel // *J. Nucl. Mater.* 2006, v. 356, p. 136-142.

11. O.V. Borodin, V.V. Bryk, A.S. Kalchenko, V.V. Melnichenko, V.N. Voyevodin, F.A. Garner. Synergistic effects of helium and hydrogen on self-ion-induced swelling of austenitic 18Cr10NiTi stainless steel // *J. Nucl. Mater.* 2013, v. 442, p. 817-820.

12. G.S. Was, Z. Jiao, E. Getto, K. Sun, A.M. Monterrosa, S.A. Maloy, O. Anderoglu, B.H. Sencer, M. Hackett. Emulation of reactor irradiation damage using ion beams *// Scr. Mater.* 2014, v. 88, p. 33-36.

13. O. Barrera, D. Bombac, Y. Chen, et al. Understanding and mitigating hydrogen embrittlement of steels: a review of experimental, modelling and design progress from atomistic to continuum // *J. Mater. Sci.* 2018, v. 53, p. 6251-6290.

14. S.K. Dwivedi, M. Vishwakarma. Hydrogen embrittlement in different materials: A review // *International Journal of Hydrogen*. 2018, v. 43, issue 46, p. 21187-21632.

15. С.А. Карпов, А.В. Никитин, Г.Д. Толстолуцкая. Деградация железа и сплавов на его основе под влиянием водородной плазмы // *Вопросы атомной науки и техники. Серия «Физика радиационных повреждений и радиационное материаловедение».* 2017, №4(110), с. 3-16.

16. S.R. Soria, A. Tolley, E.A. Sanchez. The influence of microstructure on blistering and bubble formation by He ion irradiation in Al alloys // *J. Nucl. Mater*. 2015, v. 467, p. 357-367.

17. K. Yutani, H. Kishimoto, R. Kasada, A Kimura. Evaluation of helium effects on swelling behavior of oxide dispersion strengthened ferritic steels under ion irradiation // *J. Nucl. Mater*. 2007, v. 367-370, p. 423-427.

18. G.M. Bond, D.J. Mazey, M.B. Lewis. Helium-bubble formation and void swelling in nimonic PE16 alloy under dual-ion (He+, Ni+) irradiation // *Nucl. Instrum. Methods Phys. Res. Sect. B*. 1983, v. 209-210, p. 381-386.

19. H. Ullmaier. Helium in fusion materials: High temperature embrittlement // *J. Nucl. Mater*. 1985, v. 133, p. 100-104.

20. M.I. Baskes. Recent advances in understanding helium embrittlement in metals // *MRS Bull.* 1986, v. 11, p. 14-18.

21. Jihong Chen, Liping Guo, Fengfeng Luo, Tiecheng Li, Yaoyao Ren and Jinping Suo. Synergistic Effects in Reduced-Activation Martensitic Steel Under Single and Sequential Helium/Hydrogen Ion Irradiation // *Fusion Science and Technology*. 2014, v. 66, p. 301-307.

22. Li Jiang, Qing Peng, Pengyuan Xiu, et al. Elucidating He-H assisted cavity evolution in alpha Cr under multiple ion beam irradiation // *Scripta Materialia*. 2020, v. 187, p. 291-295.

23. W-Z. Han, M-S. Ding, Z-W. Shan. Cracking behavior of helium-irradiated small-volume copper // *Scr. Mater.* 2018, v. 147, p. 1-5.

24. A. McNabb, P.K. Foster. A. A new analysis of the diffusion of hydrogen in iron and ferritic steels // *Trans. Met. Soc. AIME*. 1963, v. 227, p. 618-627.

25. S.M. Myers, S.T. Picraux et al. Defect trapping of ion-implanted deuterium in Fe // *J. Appl. Phys.* 1979, v. 50, №9, p. 5710-5719.

26. M.I. Baskes. DIFFUSE 83, Sandia, National Laboratories Report SAND83-8231. 1983.

27. S.O. Karpov, V.V. Ruzhits'ky, I.M. Neklyudov, V.I. Bendikov, G.D. Tolstoluts'ka. Parameters of trapping and the thermoactivated output of the deuterium ion-implanted into the Cr18Ni10Ti steel // *Metallofiz. Noveishie Tekhnol.* 2004, v. 26(12), p. 1661-1670 (in Russian).

28. F.A. Garner, E.P. Simonen, B.M. Oliver, L.R. Greenwood, M.L. Grossbeck, W.G. Wolfer, P.M. Scott. Retention of hydrogen in fcc metals irradiated at temperatures leading to high densities of bubbles or voids // *J. Nucl. Mater.* 2006, v. 356, p. 122-135.

29. С.А. Карпов, И.Е. Копанец, И.М. Неклюдов, В.В. Ружицкий, Г.Д. Толстолуцкая. Исследование захвата дейтерия в нержавеющих сталях 06Х18Н10, 08Х18Н10Т и 12Х18Н10Т // *Вопросы атомной науки и техники. Серия: «Физика радиационных повреждений и радиационное материаловедение»* 2005, №3(86), с. 176-178.

30. S.A. Karpov, G.D. Tolstolutskaya, B.S. Sungurov, V.V. Ruzhytskiy. Microstructure evolution and deuterium trapping in low-energy cascades after irradiation of SS316 stainless steel // *PAST*. 2017, N 2(108), p. 36-40.

31. G.D. Tolstolutskaya, V.V. Ruzhytskyi, V.N. Voyevodin, I.E. Kopanets, S.A. Karpov, A.V. Nikitin. The role of radiation damage on retention and temperature intervals of helium and hydrogen detrapping in structural materials // *J. Nucl. Mater.* 2013, v. 442, p. S710-S714.

32. S.A. Karpov, I.E. Kopanets, V.V. Ruzhytskyi, B.S. Sungurov, G.D. Tolstolutskaya. Cooperative effect of displacement damage and inert gas impurities on deuterium retention in austenitic and ferritic-martensitic steels // *PAST*. 2014. N 4(92), p. 31-37.

33. S. Myers, M. Baskes, H. Birnbaum, et al. Hydrogen interactions with defects in crystalline solids // *Rev. Mod. Phys.* 1992, v. 264, p. 559-617.

34. D. Tanguy, Y. Wang, D. Connétable. Stability of vacancy-hydrogen clusters in nickel from first-principles calculations // *Acta Materialia*. 2014, v. 78, p. 135-143.

35. A.V. Subashiev, H.H. Nee. Hydrogen trapping at divacancies and impurity-vacancy complexes in nickel: First principles study // *J. Nucl. Mater.* 2017, v. 487, p. 135-142.

36. X.-L. Zhu, Y. Zhang, L. Cheng et al. Deuterium occupation of vacancy-type defects in argon-damaged tungsten exposed to high flux and low energy deuterium plasma // *Nucl. Fusion.* 2016, v. 56, p. 036010.

37. X.-S. Kong, J. Hou, X.-Y. Li et al. First principles study of inert-gas (helium, neon, and argon) interactions with hydrogen in tungsten // *J. Nucl. Mater.* 2017, v. 487, p. 128-134.

38. Luca Chiari, Kenji Kojima, Yusuke Endo et al. Formation and time dynamics of hydrogen-induced

vacancies in nickel // *Acta Materialia*. 2021, v. 219, p. 117264.

39. L.K. Mansur, A.F. Rowcliffe, R.K. Nanstad, S.J. Zinkle, et al. Materials needs for fusion, generation IV fission reactors and spallation neutron sources – similarities and differences // *J. Nucl. Mater*. 2004, v. 329-333, p. 166-172.

40. P. Yvon, F. Carré. Structural materials challenges for advanced reactor systems // *J. Nucl. Mater.* 2009, v. 385, p. 217-222.

41. S. Zinkle, J. Busby. Structural materials for fission & fusion energy // *Mater. Today*. 2009, v. 12, p. 12-19.

42. A. Kohyama, A. Hishinuma, D.S. Gelles, R.L. Klueh, et al. Low-activation ferritic and martensitic steels for fusion application // *J. Nucl. Mater*. 1996, v. 233-237, p. 138-147.

43. A. Turk, Gaurav R. Joshi, Marius Gintalas et al. Quantification of hydrogen trapping in multiphase steels: Part I - Point traps in martensite // *Acta Materialia*. 2020, v. 194, p. 118-133.

44. A.S. Kholtobina, R. Pippan, L. Romaner, et al. Hydrogen Trapping in bcc Iron // *Materials.* 2020, v. 13, p. 2288.

45. D.A. Mirzaev, A.A. Mirzoev, K.Y. Okishev, A.V. Verkhovykh. Hydrogen–vacancy interaction in bcc iron: Ab initio calculations and thermodynamics // *Mol. Phys*. 2014, v. 112, p. 1745-1754.

46. E.J. McEniry, T. Hickel, J.J. Neugebauer. Hydrogen behaviour at twist {110} grain boundaries in α-Fe // *Philos. Trans. A Math. Phys. Eng. Sci*. 2017, v. 375, p. 20160402.

47. Y. Zhao, G. Lu. QM/MM study of dislocation–Hydrogen/helium interactions in α-Fe // *Model. Simul. Mater. Sci. Eng.* 2011, v. 19, p. 065004.

48. M. Itakura, H. Kaburaki, M. Yamaguchi, T. Okita. The effect of hydrogen atoms on the screw dislocation mobility in bcc iron: A first-principles study // *Acta Mater*. 2013, v. 61, p. 6857-6867.

49. Y. Tateyama, T. Ohno. Stability and clusterization of hydrogen-vacancy complexes in α-Fe: An ab initio study // *Phys. Rev. B*. 2003, v. 67, p. 174105.

50. T. Lu, Y.P. Xu, X.D. Pan, et al. Atomistic study of hydrogen behavior around dislocations in α iron // *J. Nucl. Mater.* 2018, v. 510, p. 219-228.

51. Ikuji Takagi, Tetsuya Komura, Masafumi Akiyoshi et al. Hydrogen traps in ion-irradiated F82H steel observed by NRA // *J. Nucl. Mater.* 2013, v. 442, p. S33-S37.

52. F. Besenbacher, S. M. Myers, P. Nordlander, J.K. Norskov. Multiple hydrogen occupancy of vacancies in Fe // *Journal of Applied Physics*. 1987, v. 61, p. 1788-1794.

53. A.V. Verkhovykh, A.A. Mirzoev, G.E. Ruzanov, D.A. Mirzaev, and K.Yu. Okishev. Interaction of hydrogen atoms with vacancies and divacancies in bcc iron // *Materials Science Forum*. 2016, v. 870, p. 550-557.

54. C. Ruset, E. Grigore, H. Maier, R. Neu, H. Greuner, M. Mayer, and G. Matthews. Development of W coatings for fusion applications // *Fusion Eng. Des*. 2011, v. 86, p. 1677-1680.

55. H. Eleveld, A. van Veen. Deuterium interaction with impurities in tungsten studied with TDS // *J. Nucl. Mater*. 1992, v. 191-194 (Part A), p. 433-438.

56. M. Poon, A.A. Haasz, J.W. Davis. Modelling deuterium release during thermal desorption of D^+-irradiated tungsten // *J. Nucl. Mater*. 2008, v. 374, p. 390-402.

57. K. Heinola, T. Ahlgren, K. Nordlund, J. Keinonen. Hydrogen interaction with point defects in tungsten // *Phys. Rev. B.* 2010, v. 82, p. 094102.

58. N. Fernandez, Y. Ferro, D. Kato. Hydrogen diffusion and vacancies formation in tungsten: Density Functional Theory calculations and statistical models // *Acta Mater*. 2015, v. 94, p. 307-318.

59. K. Ohsawa, J. Goto, M. Yamakami, M. Yamaguchi, M. Yagi. Trapping of multiple hydrogen atoms in a tungsten monovacancy from first principles // *Phys. Rev. B.* 2010, v. 82, p. 184117.

60. Y.-W. You, X.-S. Kong, X.-B. Wu, et al. Dissolving, trapping and detrapping mechanisms of hydrogen in bcc and fcc transition metals // *AIP Adv.* 2013, v. 3, p. 012118.

61. O.V. Ogorodnikova, J. Roth, M. Mayer. Ion-driven deuterium retention in tungsten // *J. Appl. Phys*. 2008, v. 103, p. 034902.

62. A. van Veen, H.A. Filius, J. de Vries, K.R. Nijkerk, G.J. Rozing, D. Segers. Hydrogen exchange with voids in tungsten observed with TDS and PA // *J. Nucl.Mater*. 1988, v. 155-57, p. 1113-1117.

63. Yu.M. Gasparyan, O.V. Ogorodnikova, V.S. Efimov, et al. Thermal desorption from self-damaged tungsten exposed to deuterium atoms // *J. Nucl. Mater*. 2015, v. 463, p. 1013-1016.

64. S. Karpov, V. Ruzhytskyi, G. Tolstolutskaya, R. Vasilenko, O. Kuprin, and S. Leonov. Thermodynamic and kinetic parameters of the processes of deuterium interaction with tungsten protective coatings // *East. Eur. J. Phys*. 2021, v. 4, p. 99-106.

65. L.M. Giancarli et al. Overview of the ITER TBM Program // *Fusion Engineering and Design*. 2012, v. 87, p. 395-402.

66. A. Vītiņš, G. Ķizāne, J. Tīliks, J. Tīliks, and E. Kolodinska. Tritium release from breeding blanket materials in high magnetic field // *Fusion Engineering and Design.* 2007, v. 82, p. 2341-2346.

67. M.H.H. Kolb, J.M. Heuser, R. Rolli, H.-C. Schneider, R. Knitter, M. Zmitko. The HICU PIE results of EU ceramic breeder pebbles: General characterization // *J. Nucl. Mater.* 2020, v. 531, p. 152023.

68. Kun Li, Wen Yang, Wei-Hua Wang, and Yong-Tang Li. First Principles Study of Tritium Diffusion in Li_2TiO_3 Crystal with Lithium Vacancy // *Materials.* 2018, v. 11, p. 2383.

69. S. Karpov, V. Ruzhytskyi, G. Tolstolutska, H. Rostova. Effect of irradiation and deuterium behavior in Li-based tritium breeding ceramics // *PAST*. 2022, N 2(138), p. 43-49.

70. K. Goswami and S. Murphy. Influence of Lithium Vacancy Defects on Tritium Diffusion in $\beta^-Li_2TiO_3$ // *J. Phys. Chem. C*. 2020, v. 124, N 23, p. 12286-12294.

71. Davide Di Stefano. *First-principles investigation of hydrogen interaction with metals*: Submitted to the

Faculty of Mathematics and Physics of the Albert-Ludwigs-Universität Freiburg im Breisgau in partial fulfillment of the requirements for the degree of a Doctor rerum naturalium. 2015, 121 p.

72. B.A. Szost, R.H. Vegter, and P.E. J. Rivera-Díaz-del Castillo. Hydrogen trapping mechanisms in nanostructured steels // *Metall. Mater. Trans.* 2013, A 44, p. 4542-4549.

73. S. Yamasaki, & T. Takahashi. Evaluation method of delayed fracture property of high strength steels // *Tetsu-to-Hagané*. 1997, v. 83, p. 454-462.

74. F.G. Wei, and K. Tsuzaki. Hydrogen absorption of incoherent TiC particles in iron from environment at high temperatures // *Metall. Mater. Trans.* 2004, v. A 35, p. 3155-3165.

75. F.G. Wei, and K. Tsuzaki. Quantitative analysis on hydrogen trapping of TiC particles in steel // *Metall. Mater. Trans.* 2006, v. A 37, p. 331-339.

76. F.G. Wei, T. Hara, and K. Tsuzaki. Precise determination of the activation energy for desorption of hydrogen in two Ti-added steels by a single thermal-desorption spectrum // *Metall. Mater. Trans.* 2004, v. B 35, p. 587-599.

77. D.P. Escobar, E. Wallaert, L. Duprez, A. Atrens, & K. Verbeken. Thermal desorption spectroscopy study of the interaction of hydrogen with TiC precipitates // *Met. Mater. Int.* 2013, v. 19, p. 741-749.

78. J. Takahashi, K. Kawakami, Y. Kobayashi, and T. Tarui. The first direct observation of hydrogen trapping sites in TiC precipitation-hardening steel through atom probe tomography // *Scr. Mater.* 2010, v. 63, p. 261-268.

79. R. Benedek et al. First principles simulation of a ceramic/metal interface with misfit // *Phys. Rev. Lett.* 2000, v. 84, p. 3362-3365.

80. F. Wei, T. Hara and K. *Tsuzaki. Nano-precipitates design with hydrogen trapping character in high strength steel*, *Advanced Steels.* Springer Berlin Heidelberg, Berlin, Heidelberg, 2011, p. 87-92.

81. J. Wei, J.H. Dong, W. Ke, X.Y. He. Influence of inclusions on early corrosion development of ultra-low carbon bainitic steel in NaCl solution // *Corrosion.* 2015, v. 71, N 12, p. 1467-1480.

82. R. Shi, Y. Ma, Z. Wang, et al. Atomic-scale investigation of deep hydrogen trapping in NbC/a-Fe semi-coherent interfaces // *Acta Materialia.* 2020, v. 200, p. 686-698.

83. Y. Chen, H. Lu, J. Liang et al. Observation of hydrogen trapping at dislocations, grain boundaries and precipitates // *Science.* 2020, v. 367, N 6474, p. 171-175.

84. G.A. Esteban, A. Peña, F. Legarda, R. Lindau. Hydrogen transport and trapping in ODS-EUROFER // *Fusion Engineering and Design*. 2007, v. 82(15), p. 2634-2640.

85. X. Hua, L. Tan, K. Wang, C.P. Massey, D.T. Hoelzer, Y. Katoh. Deuterium retention in advanced steels for fusion reactor structural application // *J. Nucl.Mater*. 2019, v. 516, p. 144-151.

86. M. Saha. Grain Boundary Segregation in Steels: Towards Engineering the Design of Internal Interfaces // *Preprints* 2022, p. 2022020096.

87. M.P. Seah. Interface adsorption, embrittlement and fracture in metallurgy. A review // *Surface Science.* 1975, v. 53, N 1. p. 168-212.

88. D. Raabe et al. Grain boundary segregation engineering in metallic alloys: A pathway to the design of interfaces // *Current Opinion in Solid State and Materials Science.* 2014, v. 18, N 4, p. 253-261.

89. C.-S. Kim, Y. Hu, G. S. Rohrer, and V. Randle. Five-parameter grain boundary distribution in grain boundary engineered brass // *Scripta Materialia.* 2005, v. 52, p. 633-637.

90. D. Raabe et al. Current Challenges and Opportunities in Microstructure-Related Properties of Advanced High-Strength Steels // *Metallurgical and Materials Transactions A: Physical Metallurgy and Materials Science.* 2020, v. 51, N 11, p. 5517-5586.

91. E.D. Hondros and C. Lea. Grain boundary microchemistry and stress-corrosion failure of mild steel // *Nature. 1981,* v. 289, N 5799, p. 663-665.

92. D. E. Spearot and M. D. Sangid. Insights on slip transmission at grain boundaries from atomistic simulations // *Current Opinion in Solid State and Materials Science.* 2014, v. 18, N 4, p. 188-195.

93. D. Brandon. 25 Year Perspective Defining grain boundaries: An historical perspective the development and limitations of coincident site lattice models // *Materials Science and Technology.* 2010, v. 26, N 7, p. 762-773.

94. D. Brandon. The structure of high-angle grain boundaries // *Acta Metallurgica.* 1966, v. 14, N 11, p. 1479-1484.

95. Xiao Zhou, Normand Mousseau, and Jun Song. Is Hydrogen Diffusion along Grain Boundaries Fast or Slow? Atomistic Origin and Mechanistic Modeling // *Physical review letters*. 2019, v. 122, p. 215501.

96. Jiaqi Li. The contribution of the grain boundary engineering to the problem of intergranular hydrogen embrittlement // *Materials*. Université de La Rochelle, 2017. ffNNT: 2017LAROS037ff. fftel01941726f.

97. H. Grimmer. Coincidence-site lattices // *Acta Crystallographica Section A.* 1976, v. 32, N 5, p. 783-785.

98. X. Sauvage, A. Ganeev, Y. Ivanisenko et al. Grain Boundary Segregation in UFG Alloys Processed by Severe Plastic Deformation // *Advanced Engineering Materials*. 2012, v. 14, N 11, p. 968-974.

99. D. Raabe et al. Metallic composites processed via extreme deformation: Toward the limits of strength in bulk materials // *MRS Bulletin*. 2010, v. 35, N 12, p. 982-991.

100. P. Lejček. Effect of Variables on Equilibrium Grain Boundary Segregation // *Springer Series in Materials Science.* 2010, p. 103-152.

101. J. Li, A. Hallil, A. Metsue, A. Oudriss, J. Bouhattate, and X. Feaugas. Antagonist efects of grain boundaries between the trapping process and the fast diffusion path in nickel bicrystals // *Scientifc Reports.* 2021, 11:15533.

102. Chase N. Taylor. Hydrogen and its detection in fusion and fission nuclear materials –a review // *J. Nucl. Mater*. 2022, v. 558, p. 153396.

103. J.B. Vetrano. Hydrides as neutron moderator and reflector materials // *Nucl. Eng. Des*. 1971, v. 14, p. 390-412.

104. A Microreactor Program Plan for The Department of Energy, INL/EXT-20-58919 (2021) 1-22.

105. DOE Microreactor Program, (2021) https://gain.inl.gov/SitePages/MicroreactorProgram.aspx (accessedOctober7,2021)

106. A. Shivprasad, T. Cutler, J. Jewell, V. Mehta, S. Paisner, C. Taylor, et al. *Advanced Moderator Material*: Handbook, 2020.

107. A.T. Motta, L. Capolungo, L.Q. Chen, M.N. Cinbiz, M.R. Daymond, D.A. Koss, et al. Hydrogen in zirconium alloys: a review // *J. Nucl. Mater*. 2019, v. 518, p. 440–460.

108. M. Blat, L. Legras, D. Noel, H. Amanrich. Contribution to a Better Understanding of the Detrimental Role of Hydrogen on the Corrosion Rate of Zircaloy- 4 Cladding Materials // *Zirconium in the Nuclear Industry: Twelfth International Symposium*, West Conshohocken, PA, ASTM International, 2000, p. 563-591.

109. D.J. Edlund, J. McCarthy. The relationship between intermetallic diffusion and flux decline in composite-metal membranes: implications for achieving long membrane lifetime // *J. Memb. Sci.* 1995, v. 107, p. 147-153.

110. L. Tournadre, F. Onimus, J.L. Béchade, D. Gilbon, J.M. Cloué, J.P. Mardon, et al. Toward a better understanding of the hydrogen impact on the radiation induced growth of zirconium alloys // *J. Nucl. Mater*. 2013, v. 441, p. 222-231.

111. S. Yagnik, R. Adamson, G. Kobylyansky, J.-H. Chen, D. Gilbon, S. Ishimoto, et al. *Effect of Alloying Elements, Cold Work, and Hydrogen on the Irradiation-Induced Growth Behavior of Zirconium Alloy*: Variants, in: R. Comstock, A. Motta (Eds.), Zirconium in the Nuclear Industry: 18th International Symposium T2, West Conshohocken, PA, Eds., ASTM International, 2018, p. 748-795.

112. Aaron W. Colldeweih, Johannes Bertsch. Effect of temperature and hydrogen concentration on the threshold stress intensity factor of radial delayed hydride cracking in fuel cladding // *J. Nucl. Mater.* 2022, v. 565, p. 153737.

113. G.D. Tolstolutskaya, I.E. Kopanets, V.V. Ruzhitsky, V.A. Belous, A.S. Kuprin, V.D. Ovcharenko, R.L. Vasilenko, S.A. Leonov. Reduction of hydrogen saturation of zirconium alloys using a modification of the surface due to complex ion-plasma treatment // *PAST*. 2015, N 2(96), p. 119-123.

114. B.W. Zhang, S.J. Hao, J.S. Wu, et al. Direct evidence of passive film growth on 316 stainless steel in alkaline solution // *Mater. Charact*. 2017, v. 131, p. 168-174.

115. L.Q. Guo, S.X. Qin, B.J. Yang, D. Liang, L.J. Qiao. Effect of hydrogen on semi-conductive properties of passive film on ferrite and austenite phases in a duplex stainless steel // *Sci. Rep*. 2017, v. 7, p. 3317-3312.

116. H. Luo, Z.M. Li, Y.H. Chen, D. Ponge, M. Rohwerder, D. Raabe. Hydrogen effects on microstructural evolution and passive film characteristics of a duplex stainless steel // *Electrochem. Commun*. 2017, v. 79, p. 28-32.

117. L.J. Dong, Q.J. Peng, Z.M. Zhang, et al. Effect of dissolved hydrogen on corrosion of 316NG stainless steel in high temperature water // *Nucl. Eng. Des*. 2015, v. 295, p. 403-414.

118. S.H. Jeon, E.H. Lee, D.H. Hur. Effects of dissolved hydrogen on general corrosion behavior and oxide films of alloy 690TT in PWR primary water // *J. Nucl. Mater*. 2017, v. 485, p. 113-121.

119. R.H. Cao, L.N. Xu, B.L. Jiang, et al. Coupling effect of microstructure and hydrogen absorbed during service on pitting corrosion of 321 austenitic stainless steel weld joints // *Corros. Sci.* 2020, v. 164, p. 108339.

120. W. Li, R. Cao, L. Xu et al. The role of hydrogen in the corrosion and cracking of steels: A review // *Corrosion Communications*. 2021, v. 4, p. 23-32.

121. Xiazi Xiao. Fundamental Mechanisms for Irradiation-Hardening and Embrittlement: A Review // *Metals.* 2019, v. 9, p. 1132-1152.

122. A. Lupinacci, K. Chen, Y. Li, et al. Characterization of ion beam irradiated 304 stainless steel utilizing nanoindentation and Laue microdiffraction // *J. Nucl. Mater*. 2015, v. 458, p. 70-76.

123. S.A. Karpov, G.D. Tolstolutskaya, B.S. Sungurov, et al. Hardening of SS316 Stainless Steel Caused by the Irradiation with Argon Ions // *Materials Science*. 2016, v. 52, issue 3, p. 377-384.

124. P.P. Liu, W.T. Han, X.O. Yi, Q. Zhan, F.R. Wan. Effect of He and H synergy on mechanical property of ion-irradiated Fe-10Cr alloy // *Fusion Engineering and Design*. 2018, v. 129, p. 221-229.

125. Y. Zhao, M.-Y. Seok, D.-H. Lee et al. Hydrogen-induced softening in nanocrystalline Ni investigated by nanoindentation // *Phil. Mag.* 2016, v. 96, issue 32-34, p. 3442-3450.

126. Q.M. Wei, N. Li, K. Sun, L.M. Wang. The shape of bubbles in He-implanted Cu and Au // *Scr. Mater*. 2010, v. 63, p. 430-433.

127. H. Iwakiri, K. Yasunaga, K. Morishita, N. Yoshida. Microstructure evolution in tungsten during low-energy helium ion irradiation // *J. Nucl. Mater*. 2000, v. 283-287, p. 1134-1138.

128. M.A. Tunes, R.W. Harrison, G. Greaves, J.A. Hinks, S.E. Donnelly. Effect of He implantation on the microstructure of zircaloy-4 studied using in situ TEM // *J. Nucl. Mater*. 2017, v. 493, p. 230-238.

129. H.H. Shen, S.M. Peng, B. Chen et al. Helium bubble evolution in a Zr-Sn-Nb-Fe-Cr alloy during post-annealing: An in-situ investigation // *Mater. Charact*. 2015, v. 107, p. 309-316.

130. G.D. Tolstolutskaya. *Mechanisms of radiation damage of the surface layers of solids under the bombardment by ions of inert gases and hydrogen*: Thesis for D. Sc. Degree in physics and mathematics. Kharkov, 2009, 330 p.

131. V.F. Zelenskij, I.M. Nekludov, V.F. Rybalko, V.V. Ruzhytskiy, V.I. Bendikov, S.M. Khazan. Thermal desorption of helium from polycrystalline Ni irradiated to fluences ranging from $1 \cdot 10^{17}$ to $1 \cdot 10^{18}$ $He^{+} \cdot cm^{-2}$ // *J. Nucl. Mater*. 1987, v. 151, N 1, p. 22-33.

132. J.L. Wang, L.L. Niu, X.L. Shu, Y. Zhang. Energetics and kinetics unveiled on helium cluster growth in tungsten // *Nucl. Fusion*. 2015, v. 55, p. 092003.

133. X.C. Li, X.L. Shu, P. Tao, et al. Molecular dynamics simulation of helium cluster diffusion and bubble formation in bulk tungsten // *J. Nucl. Mater*. 2014, v. 455, p. 544-548.

134. N. Gao, M. Victoria, J. Chen, H.V. Swygenhoven. H.V. Helium-vacancy cluster in a single bcc iron crystal lattice // *J. Phys. Condens. Matter*. 2011, v. 23, p. 245403.

135. R. Kobayashi, T. Hattori, T. Tamura, S. Ogata. A molecular dynamics study on bubble growth in tungsten under helium irradiation // *J. Nucl. Mater*. 2015, v. 463, p. 1071-1074.

136. L. Sandoval, D. Perez, B.P. Uberuaga, A.F. Voter. Formation of helium-bubble networks in tungsten // *Acta Mater*. 2018, v. 159, p. 46-50.

137. S.H. Guo, B.E. Zhu, W.C. Liu, Z.Y. Pan, Y.X. Wang. Pressure of stable He-vacancy complex in bcc iron: Molecular dynamics simulations // *Nucl. Instrum. Methods Phys. Res. B.* 2009, v. 267, p. 3278-3281.

138. H.B. Zhou, Y.L. Liu, Y. Zhang, S. Jin, G.H. Lu. First-principles investigation of energetics and site preference of He in a W grain boundary // *Nucl. Instrum. Methods Phys. Res. B.* 2009, v. 267, p. 3189-3192.

139. L. Ventelon, F. Willaime, C.C. Fu, M. Heran, I. Ginoux. Ab initio investigation of radiation defects in tungsten: Structure of self-interstitials and specificity of di-vacancies compared to other bcc transition metals // *J. Nucl. Mater*. 2012, v. 425, p. 16-21.

140. W. Xiao, X. Zhang, W.T. Geng, G. Lu. Helium bubble nucleation and growth in α-Fe: Insights from first–principles simulations // *J. Phys. Condens. Matter*. 2014, v. 26, p. 255401.

141. M. Samaras. Multiscale Modelling: The role of helium in iron // *Mater. Today*. 2009, v. 12, p. 46-53.

142. C.S. Becquart, C. Domain. Migration energy of He in W revisited by ab initio calculations // *Phys. Rev. Lett*. 2006, v. 97, p. 196402.

143. T. Seletskaia, Y. Osetsky, R.E. Stoller, G.M. Stocks. Magnetic interactions influence the properties of helium defects in iron // *Phys. Rev. Lett*. 2005, v. 94, p. 046403.

144. G.Y. Huang, N. Juslin, B.D.Wirth. First-principles study of vacancy, interstitial, noble gas atom interstitial and vacancy clusters in bcc-W // *Computational Materials Science.* 2016, v. 123, p. 121-130.

145. L. Yang, H.Q. Deng, F. Gao, et al. Atomistic studies of nucleation of He clusters and bubbles in bcc iron // *Nucl. Instrum. Methods Phys. Res. B*. 2013, v. 303, p. 68-71.

146. Lei Wan, Xiaoqiu Ye, Xingzhong Cao, Shuoxue Jin, Tao Gao. First-principles study of helium in austenitic Fe 6.3 at% Cr alloys: Structural, stability, energetics, and clustering with vacancies // *Mater. Today Com*. 2021, v. 29, p. 102837.

147. T. Seletskaia, Y. Osetsky, R.E. Stoller, G.M. Stocks. Calculation of helium defect clustering properties in iron using a multi-scale approach // *J. Nucl. Mater*. 2006, v. 351, p. 109-118.

148. F. Gao, H.Q. Deng, H.L. Heinisch, R.J. Kurtz. A new Fe–He interatomic potential based on ab initio calculations in a-Fe // *J. Nucl. Mater*. 2011, v. 418, p. 115-120.

149. W.D. Wilson, R.A. Johnson. Rare gases in metals // *Proceedings of the Battelle Institute Materials Science Colloquia*, Columbus, OH, USA, 17 September 1972, p. 375-390.

150. D.M. Stewart, Y.N. Osetsky, R.E. Stoller, et al. Atomistic studies of helium defect properties in bcc iron: Comparison of He–Fe potentials // *Phil. Mag*. A 2010, v. 90, p. 935-944.

151. P.H. Chen, X.C. Lai, K.Z. Liu, et. al. Development of a pair potential for Fe–He by lattice inversion // *J. Nucl. Mater*. 2010, v. 405, p. 156-159.

152. K. Morishita, R. Sugano, B.D. Wirth. MD and KMC modeling of the growth and shrinkage mechanisms of helium–vacancy clusters in Fe // *J. Nucl. Mater*. 2003, v. 323, p. 243-250.

153. R. Kobayashi, T. Hattori, T. Tamura, and S. Ogata. A molecular dynamics study on bubble growth in tungsten under helium irradiation // *J. Nucl. Mater*. 2015, v. 463, p. 1071-1074.

154. L. Sandoval, D. Perez, B.P. Uberuaga, A.F. Voter. Competing kinetics and He bubble morphology in W // *Phys. Rev. Lett*. 2015, v. 114, p. 105502.

155. L. Yang et al. Effects of local structure on helium bubble growth in bulk and at grain boundaries of bcc iron: A molecular dynamics study // *Acta Mater*. 2015, v. 97, p. 86-93.

156. H.X. Xie, N. Gao, K. Xu, et.al. A new loop-punching mechanism for helium bubble growth in tungsten // *Acta Mater*. 2017, v. 141, p. 10-17.

157. H. Trinkaus and W. Wolfer. Conditions for dislocation loop punching by helium bubbles // *J. Nucl. Mater*. 1984, v. 122(1-3), p. 552-557.

158. W. Wolfer. The pressure for dislocation loop punching by a single bubble // *Philos. Mag*. 1988, v. A 58(2), p. 285-297.

159. H. Trinkaus, B.N. Singh. Helium accumulation in metals during irradiation. Where do we stand? // *J. Nucl. Mater*. 2003, v. 323, p. 229-242.

160. N. Marochov, L.J. Perryman, P.J. Goodhew. Growth of inert gas bubbles after implantation // *J. Nucl. Mater*. 1987, v. 149, p. 296-301.

161. P.J. Goodhew, S.K. Tyler. Helium bubble behaviour in b.c.c. metals below $0.65T_m$ // *Proc. R. Soc. Lond. Ser. A*. 1981, v. 377, 151-184.

162. B.N. Singh, H. Trinkaus. An analysis of the bubble formation behaviour under different experimental conditions // *J. Nucl. Mater*. 1992, v. 186, 153-165.

163. A.J. Markworth. On the coarsening of gas-filled pores in solids // *Metall. Trans. A*. 1973, v. 4, p. 2651-2656.

164. G.W. Greenwood, A. Boltax. The role of fission gas re-solution during post-irradiation heat treatment // *J. Nucl. Mater*. 1962, v. 5, p. 234-240.

165. K. Ono, K. Arakawa, M. Oohashi, H. Kurata, K. Hojou, N. Yoshida. Formation and migration of helium bubbles in Fe–16Cr–17Ni austenitic alloy at high temperature // *J. Nucl. Mater*. 2000, v. 283-287, p. 210-214.

166. V.I. Bendikov, A.V. Nikitin, V.V. Ruzhytskyi, V.F. Rybalko, S.M. Khazan. Thermal desorption of helium from polycrystalline Ni // *PAST. Series "Physics*

of Radiation Effects and Radiation Materials Science". 1996, N 1(64), p. 65-71.

167. V.V. Ruzhytskyi, S.A. Karpov, A.S. Kalchenko, I.E. Kopanets, B.S. Sungurov, G.D. Tolstolutskaya. Helium porosity development during annealing of helium-implanted 18Cr10NiTi steel // *East Eur. J. Phys*. 2018, v. 4, 69-76.

168. J. Rothaut, H. Schroeder & H. Ullmaier. The growth of helium bubbles in stainless steel at high temperatures // *Philos. Mag. A.* 1983, v. 47, p. 781-795.

169. K. Ono, K. Arakawa, K. Hojou. Formation and migration of helium bubbles in Fe and Fe-9Cr ferritic alloy // *J. Nucl. Mater*. 2002, v. 307-311, p. 1507-1512.

170. A.S. Kalchenko, S.A. Karpov, I.E. Kopanets, M.A. Tikhonovsky, G.D. Tolstolutskaya. Comparative study of helium bubble formation in Cr-Fe-Ni-Mn high-entropy alloy and 18Cr10NiTi steel after irradiation and post-irradiation annealing // *Problems of Atomic Science and Technology*. 2019, v. 5, p. 25-29.

171. M. Roldan, P. Fernandez, J. Rams, F.J. Sanchez, A. Gomez-Herrero. Nanoindentation and TEM to study the cavity fate after post-irradiation annealing of He implanted EUROFER97 and EU-ODS EUROFER // *Micromachines*. 2018, v. 9, p. 633-639.

172. Y. Dai, G.R. Odette, and T. Yamamoto. The Effects of Helium in Irradiated Structural Alloys // *Comprehensive Nuclear Materials* / Editors R. Konings and R. Stoller. 2nd edition (Amsterdam: Elsevier), v. 1, p. 186-234.

173. J. Marian, T. Hoang, M. Fluss, and L.L. Hsiung. A Review of Helium-Hydrogen Synergistic Effects in Radiation Damage Observed in Fusion Energy Steels and an Interaction Model to Guide Future Understanding // *J. Nucl. Mater.* 2015, v. 462, p. 409-421.

174. K. Farrell and E. Lee. Ion Bombardment Damage in a Modified Fe-9Cr-1Mo Steel // *Philadelphia: American Society for Testing and Materials*. 1985, p. 383-393.

175. E. Wakai, T. Sawai, K. Furuya, A. Naito, T. Aruga, K. Kikuchi, S. Yamashita, S. Ohnuki, S. Yamamoto, H. Naramoto, S. Jistukawa. Effect of triple ion beams in ferritic/martensitic steel on swelling behavior // *J. Nucl. Mater*. 2002, v. 307-311, p. 278-282.

176. E. Wakai, K. Kikuchi, S. Yamamoto, et al. Swelling behavior of F82H steel irradiated by triple/dual ion beams // *J. Nucl. Mater*. 2003, v. 318, p. 267-273.

177. E. Wakai, M. Ando, T. Sawai, et al. Effect of gas atoms and displacement damage on mechanical properties and microstructures of F82H // *J. Nucl. Mater*. 2006, v. 356, p. 95-104.

178. E. Wakai, M. Ando, T. Sawai, S. Ohnuki. Effect of helium and hydrogen production on irradiation hardening of F82H steel irradiated by ion beams // *Mater. Trans*. 2007, v. 48, p. 1427-1430.

179. K. Farrell and E. Lee. Ion Damage in a Fe-10Cr-6Mo-0.5Nb Ferritic Steel // *Philadelphia: American Society for Testing and Materials.*1987, p. 498-507.

180. N. Sekimura, T. Iwai, Y. Arai, et al. Synergistic Effects of Hydrogen and Helium on Microstructural Evolution in Vanadium Alloys by Triple Ion Beam Irradiation // *J. Nucl. Mater.* 2000, v. 283-287, p. 224-228.

181. T. Tanaka, K. Oka, S. Ohnuki, et al. Synergistic Effect of Helium and Hydrogen for Defect Evolution under Multi-Ion Irradiation of Fe-Cr Ferritic Alloys // *J. Nucl. Mater*. 2004, v. 329-333, p. 294-298.

182. O.V. Borodin, V.V. Bryk, A.S. Kalchenko, V.V. Melnichenko, V.N. Voyevodin, and F.A. Garner. Synergistic Effects of Helium and Hydrogen on Self-Ion-Induced Swelling of Austenitic 18Cr10NiTi Stainless Steel // *J. Nucl. Mater*. 2013, v. 442, p. S817-S820.

183. D. Brimbal, L. Beck, O. Troeber, E. Gaganidze, et al. Microstructural Characterization of Eurofer-97 and Eurofer-ODS Steels before and after Multi-Beam Ion Irradiations at JANNUS Saclay Facility // *J. Nucl. Mater*. 2015, v. 465, p. 236-244.

184. H. Liu, J. Huang, L. Cao, et al. Helium-hydrogen Synergistic Effects on Swelling in In-Situ Multiple-Ion Beams Irradiated Steels // *Chin. Phys*. 2021, v. B 30 (8), p. 086106.

185. L. Jiang, Q. Peng, P. Xiu, et al. Elucidating He-H Assisted Cavity Evolution in Alpha Cr under Multiple Ion Beam Irradiation // *Scr. Mater*. 2020, v. 187, p. 291-295.

186. K. Farrell, M.B. Lewis, and N.H. Packan. Simultaneous Bombardment with Helium, Hydrogen, and Heavy Ions to Simulate Microstructural Damage from Fission or Fusion Neutrons // *Scr. Metal*. 1978, v. 12 (12), p. 1121-1124.

187. S. Hamada, Y.C. Zhang, Y. Miwa, and D. Yamaki. Effect of Triple Beam Irradiation on Microstructural Evolution in Austenitic Stainless Steel // *Radiat. Phys. Chem*. 1997, v. 50 (6), p. 555-559.

188. Y.E. Kupriiyanova, V.V. Bryk, O.V. Borodin, et al. Use of Double and Triple-Ion Irradiation to Study the Influence of High Levels of Helium and Hydrogen on Void Swelling of 8–12% Cr Ferritic-Martensitic Steels // *J. Nucl. Mater.* 2016, v. 468, p. 264-273.

189. N. Zimber, P. Vladimirov, M. Klimenkov, et al. Microstructural Evolution of Three Potential Fusion Candidate Steels under Ion-Irradiation // *J. Nucl. Mater*. 2020, v. 535, p. 152160.

190. M. Roldán, P. Fernández, R.Vila, et al. The Effect of Triple Ion Beam Irradiation on Cavity Formation on Pure EFDA Iron // *J. Nucl. Mater*. 2016, v. 479, p. 100-111.

191. K. Farrell, P.J. Maziasz, E.H. Lee, L.K. Mansur. Modification of Radiation Damage Microstructure By Helium // *Radiat. Eff.* 1983, v. 78, p. 277-295.

192. R.E. Stoller. The influence of helium on microstructural evolution: Implications for DT fusion reactors // *J. Nucl. Mater*. 1990, v. 174, p. 289-310.

193. Y. Katoh, M. Ando, A. Kohyama. Radiation and helium effects on microstructures, nano-indentation properties and deformation behavior in ferrous alloys // *J. Nucl. Mater*. 2003, v. 323, p. 251-262.

194. Y.R. Lin, A. Bhattacharya, D. Chen, J.J. Kai, J. Henry, S.J. Zinkle. Temperature-dependent cavity swelling in dual-ion irradiated Fe and Fe-Cr ferritic alloys // *Acta Mater.* 2021, v. 207, p. 116660.

195. A. Molvik, A. Ivanov, G.L. Kulcinski, et al. A Gas Dynamic Trap Neutron Source for Fusion Material and Subcomponent Testing // *Fusion Sci. Techn.* 2010, v. 57 (4), p. 369-394.

196. A. Kohyama, G. Ayrault, N. Igata. Microstructural evolution in dual-ion irradiated 316ss under

various helium injection schedules // *J. Nucl. Mater*. 1984, v. 122 (1), p. 224-229.

197. K. Farrell. Experimental effects of helium on cavity formation during irradiation: A review // *Radiat. Eff*. 1980, v. 53 (3-4), p. 175-194.

198. A. Bhattacharya and S.J. Zinkle. Cavity Swelling in Irradiated Materials // *Comprehensive Nuclear Materials* / Editors R. Konings and R. Stoller. 2nd edition, Amsterdam: Elsevier. 2020, v. 1, p. 406-455.

199. J. Chen, L. Guo, F. Luo, et al. Synergistic Effects in Reduced-Activation Martensitic Steel under Single and Sequential Helium/Hydrogen Ion Irradiation // *Fusion Sci. Techn*. 2017, v. 66 (2), p. 301-307.

200. P. Jin, T. Shen, M. Cui, et al. Study on Vacancy-type Defects in SIMP Steel Induced by Separate and Sequential H and He Ion Implantation // *J. Nucl. Mater*. 2019, v. 520, p. 131-139.

201. J.D. Hunn, E.H. Lee, T.S. Byun, L.K. Mansur. Helium and hydrogen induced hardening in 316LN stainless steel // *J. Nucl. Mater*. 2000, v. 282 (2-3), p. 131-136.

202. P. Jin, T.L. Shen, J. Li, et al. Spherical nanoindentation stress–strain responses of SIMP steel to synergistic effects of irradiation by H and He ions // *Nucl. Sci. Tech*. 2022, v. 33, p. 6.

203. R.E. Stoller, G.R.Odette. Analytical solutions for helium bubble and critical radius parameters using a hard sphere equation of state // *J. Nucl. Mater*. 1985, v. 131 (2-3), p. 118-125.

204. S. Lee, S. Myers, R. Spulak. Trapping of deuterium by helium bubbles and defects in ion-implanted tantalum // *J. Appl. Phys*. 1989, v. 66, p. 1137-1246.

205. E. Abramov, D. Eliezer. Hydrogen trapping in helium damaged metals: a theoretical approach // *J. Mater. Sci*. 1992, v. 27, p. 2595-2598.

206. S.M. Myers, F. Besenbacher, J. Bottiger. Deuterium in He-implanted Fe: Trapping and the surface permeation barrier // *Appl. Phys. Lett*. 1981, v. 39, p. 450-452.

207. J.P. Hirth. Effects of hydrogen on the properties of iron and steel // *Metall. Trans. A*. 1980, v. 11, p. 861-890.

208. M. Blackmur, S. Dumbill, I. MacLaren, et al. The association of hydrogen with nanometre bubbles of helium implanted into zirconium // *Scr. Mater*. 2018, v. 152, p. 102-106.

209. N. Juslin, B.D. Wirth. Molecular dynamics simulation of the effect of sub-surface helium bubbles on hydrogen retention in tungsten // *J. Nucl. Mater*. 2013, v. 438, p. S1221-S1223.

210. S.A. Karpov, G.D. Tolstolutskaya, A.S. Kalchenko. Effect of noble-gas bubbles on deuterium trapping behavior in argon pre-implanted stainless steel // *J. Nucl. Mater*. 2022, v. 566, p. 153661.

211. F.A. Garner, E.P. Simonen, B.M. Oliver, L.R. Greenwood, M.L. Grossbeck, W.G. Wolfer, P.M. Scott. Retention of hydrogen in fcc metals irradiated at temperatures leading to high densities of bubbles or voids // *J. Nucl. Mater*. 2006, v. 356, p. 122-135.

212. J. Hou, X.-S. Kong, X. Wu, J. Song, C. Liu. Predictive model of hydrogen trapping and bubbling in nanovoids in bcc metals // *Nature Mater*. 2019, v. 18, p. 833-839.

213. E. Hayward and Chu-Chun Fu. Interplay between hydrogen and vacancies in α-Fe // *Phys. Rev. B.* 2013, v. 87, p. 174103.

214. E. Hayward and C. Deo. Synergistic effects in hydrogen–helium bubbles // *J. Phys.: Condens. Matter*. 2012, v. 24, p. 265402.

215. L.N. Clowers, Z. Jiao, G.S.Was. Synergies between H, He and radiation damage in dual and triple ion irradiation of candidate fusion blanket materials // *J. Nucl. Mater*. 2022, v. 565, p. 153722.

216. C.D. Judge, H. Rajakumar, A. Korinek, G.A. Bickel. On the Potential Synergies of Helium and Hydrogen on the Nucleation and Stability of Cavity Clusters in Inconel X-750 Irradiated in a High Thermal Neutron Flux Spectra // *19th Int Conf. Environ. Degrad. Mater. Nucl. Power Syst. – Water React. EnvDeg*. 2019, p. 688-694.

217. D. Brimbal, L. Beck, M. Payet, F. Jomard. The synergistic effect of hydrogen and helium implantations in forming H_2 molecules in a Fe-12 wt.% Cr-ODS steel characterized by Raman spectroscopy and SIMS // *Nucl. Instr. Meth. in Phys. Res. B*. 2019, v. 461, p. 191-196.

Article received 18.05.2022

ЕФЕКТИ ГЕЛІЮ ТА ВОДНЮ В КОНСТРУКЦІЙНИХ МАТЕРІАЛАХ ДЛЯ ЯДЕРНИХ ЗАСТОСУВАНЬ

С.О. Карпов, Г.Д. Толстолуцька

У реакторних умовах каскади зміщення генерують безліч радіаційних дефектів, але особливе занепокоєння викликає одночасне утворення гелію (He) та водню (H), які посилюють деградацію конструкційних матеріалів. Переважна більшість виконаних досліджень щодо взаємодії гелію та водню з матеріалами заснована на іонно-пучковому опроміненні, яке є зручним інструментом для моделювання впливу нейтронів у різних температурних та дозових режимах завдяки можливості широко варіювати та контролювати параметри опромінення. В огляді обговорюються експериментальні дослідження взаємодії водень-дефект, виконані методом термодесорбційної спектроскопії, а також параметри цієї взаємодії, отримані шляхом чисельних розрахунків, заснованих на моделюванні дифузійного захоплення. Ми також узагальнюємо попередні дослідження з вивчення впливу меж зерен та нанопреципітатів на перенесення водню в металах, а також впливу водню на корозію та розтріскування сталей. Крім того, обговорюються питання утворення бульбашок гелію та деякі свідчення синергетичного ефекту водню та гелію у присутності пошкоджень зміщення, а також їх вплив на радіаційне зміцнення та розпухання. Особливу увагу приділено особливостям взаємодії водню з бульбашками інертних газів, розглянутим з урахуванням останніх опублікованих даних.